A 2.5D coupled FEM-BEM-MFS methodology for longitudinally invariant soil-structure interaction problems

Hassan Liravi[a,*], Robert Arcos[a,b], Dhananjay Ghangale[a], Behshad Noori[c], Jordi Romeu[a]

[a]*Acoustical and Mechanical Engineering Laboratory (LEAM), Universitat Politècnica de Catalunya (UPC). c/ Colom, 11, 08222 Terrassa (Barcelona), Spain.*
[b]*Serra Húnter Fellow, Universitat Politècnica de Catalunya (UPC).*
[c]*AV Ingenieros, C/ Joan XXIII, 23. 08173 St. Cugat del Vallès (Barcelona), Spain.*

Abstract

This paper is concerned with a new prediction methodology for longitudinally invariant soil-structure interaction problems in elastodynamics. The method uses the finite-element method to model the structure, the boundary-element method to model the local soil surrounding the structure and the method of fundamental solutions to model the wave propagation through the soil, all of them formulated in the two-and-a-half dimensional domain. The proposed method firstly obtains the displacement field on the soil-structure interaction boundary making use of a two-and-a-half dimensional coupled finite element-boundary element method. The method of fundamental solutions is used then as a post-processing tool to compute the response of the soil, increasing the computational efficiency of the overall methodology with respect to a methodology that considers the boundary element method as a model of the wave propagation through the soil. The accuracy of the methodology is verified for four calculation examples: a solid cylinder and a circular thin shell embedded in a homogeneous full-space and also in a homogeneous half-space. This verification is performed comparing the results with available analytical or semi-analytical solutions and a conventional two-and-a-half dimensional coupled finite element-boundary element method. Furthermore, a control methodology to increase the robustness of the method is presented.

Keywords: Method of fundamental solutions; 2.5D FEM-BEM-MFS; Elastodynamics; Soil-structure interaction; Mesh-free methods; Homogeneous full-space and half-space problems.

1. Introduction

A large variety of numerical methods are provided by the literature for dynamic assessment of soil-structure interaction problems. This area of research is actively bringing new mesh-based methodologies to study soil-structure interaction problems related to different types of engineering structures [5]. Some of these soil-structure interaction problems are addressed within the consideration that they are longitudinally invariant systems, as for example the cases of railway infrastructures, roads and pipelines. For this kind of systems, two-and-a-half dimensional (2.5D) modelling approaches [22, 17] are found to be a better alternative than three dimensional (3D) models [3]. Sheng et al. [27] presented an approach based on the finite element-boundary element method (FEM-BEM) for railway-induced ground-borne vibration problems. Lopes et al. studied the influence of soil stiffness on soil-structure interaction using a 2.5D FEM-PML approach [23]. Other investigations [9, 10] proposed a method to use the Green's functions of a layered half-space [25] as Green's functions used in BEM, leading to significant simplifications of the meshing problem. An interesting alternative approach for obtaining the Green's functions required in 2.5D BEM in elastodynamics is the thin layer method [6]. From another perspective, various semi-analytical approaches were developed to deal with 2.5D soil-structure dynamic interaction problems. In the case of tunnel-soil systems, a well-established method on the field is the Pipe-in-Pipe (PiP) model [7, 8, 19], a method that ensures accurate results only when the tunnel is deeply

*Corresponding Author
Email addresses: Hassan.liravi@upc.edu

buried on the ground. More recently, a semi-analytical solution for the case of a tunnel embedded in a multi-layered half-space that overcomes the PiP limitation were presented by He and his colleagues [16]. This method ensures highly accurate results but its formulation is mathematically complex. Nevertheless, these semi-analytical approaches are limited to very simple geometries of the tunnel structure.

However, to avoid the constraints due to mesh-based approaches and increasing the computational efficiency of the solutions, the method of fundamental solutions (MFS), as a mesh-free and integration-free approach, has been proposed to estimate values inside the domain. This method can be applied effectively in elastodynamic problems, as shown in [29]. Later, methodologies that combine MFS with mesh-based approaches to deal with soil-structure interaction problems have been developed. Godinho et al. [13] presented two-dimensional FEM-MFS modelling approach for these types of problems. An extension of this to longitudinally invariant systems was presented by Amado-Mendes and his colleagues [2], where a methodology that models the structure using 2.5D FEM and the surrounding soil with 2.5D MFS is proposed. Godinho et al. [14] presented a fully meshless method to deal with soil-structure interaction problems in the frequency domain where the MFS is used to model the soil while the meshless local Petrov–Galerkin method is used to model the structure. More recently, Ghangale et al. [12, 11] presented a novel numerical methodology for the prediction of the vibration energy flow radiated by an underground railway system that uses a 2.5D FEM-BEM approach to model a railway tunnel and its surrounding ground and, then, uses the semi-analytical solutions of a cavity embedded in a full-space to model the wave propagation on the soil.

MFS is a meshless method that employs the fundamental solution of the governing equation of interest as the interpolation basis function. It is specially interesting for dealing with wave propagation problems in unbounded or partially unbounded domains. Its application is based on a distribution of collocation points, which evaluates the boundary conditions at discrete positions, and on a distribution of source points (or virtual forces, in elastodynamic problems), which are obtained by complying the boundary condition at the collocation points. The collocation points are located on the boundary and the source points outside the domain. For many years, it has been a concern of the researchers to find the optimal distance between collocation and source points, particularly in complicated shapes. An incorrect selection of this distance may lead to large errors of the numerical method [1]. Besides, it should be noted that the amount of source points affects the numerical convergence and stability of the results [28]. Chen et al. [4] proposed to minimise the error of the MFS through two algorithms. They considered one algorithm that minimises the error on the boundary condition satisfaction and the leave-one-out cross-validation (LOOCV) algorithm to find the optimal position of the virtual source points. Furthermore, Wong et al. [32] showed that there is a strong relation between the optimal position and density of the virtual source points and the effective-condition-number, which thus can be used to optimise the virtual sources distribution. The need of an optimal determination of the distance between collocation points and virtual sources belongs to the inherent numerical instability of the MFS. Various numerical phenomena make it inaccurate and unstable: The singularity of ill-conditioned matrices [18, 24] or ill-posed problems [31] are the most common numerical issues associated to the MFS application.

In the current paper, a 2.5D FEM-BEM-MFS approach in Cartesian coordinates and in the frequency domain is presented. The method uses 2.5D MFS as a post-processing tool to obtain the displacement and traction fields on the soil from the displacement field on the soil-structure interaction boundary. That displacement field on the boundary is proposed to be obtained by using a 2.5D FEM-BEM approach. The main novelty of the current paper is, thus, the way MFS is applied, which leads to two global benefits. On one hand, the application of this methodology results to an increase of the computational efficiency of the method respect to traditional 2.5D FEM-BEM approaches [9], and that mostly matters when many evaluation points are required to be analysed. On the other hand, a substantial difference between the work of Amado-Mendes et al. [2] and the method proposed here is related about how the dynamic stiffness matrix of the soil at the soil-structure interaction boundary is obtained: Amado-Mendes work uses the MFS while the present method uses the BEM. Since BEM discretises the boundary in elements instead on the discrete collocation points appearing in MFS, the methodology presented here ensures higher accuracy on the computation of the displacement and traction fields on the soil-structure interaction boundary, which results in a significant reduction of the errors associated to the displacement and traction fields on the soil. As shown in this article, this is of special importance for the traction field on the soil, since it has a stronger dependency on the accuracy of the displacement and traction fields on the boundary. In terms of computational efficiency, 2.5D FEM-MFS generally overcomes the proposed method since it avoids the integration along the boundary required in BEM. However, this paper demonstrates that the new proposed method is specially relevant for large amounts of evaluation points: in these cases, both 2.5D FEM-MFS and 2.5D FEM-BEM-MFS methods exhibit very similar levels of efficiency. Also, in this

work, an interpolation-based technique that considerably increases the accuracy/efficiency of the method is studied. In this technique, the values on the boundary obtained by 2.5D FEM-BEM are interpolated to have more collocation points to be used in the MFS. All of these capabilities lead to a comprehensive method which takes the robustness of FEM-BEM approaches combined with the computational efficiency of the MFS. The methodology is tested and verified for homogeneous full-space and half-space cases for two structures: a solid and a cavity embedded on the soil. Finally, the present work proposes an error detection tool to control the error of the displacement and traction fields on the soil, ensuring the robustness of the methodology. This control technique is based on control points in the field fully evaluated by the 2.5D FEM-BEM. These control points can be used to find the location of the virtual sources that optimises the MFS performance in terms of accuracy. This is a new feature as compared with the 2.5D FEM-MFS method.

2. Numerical method

A general description of the methodology developed in the current article is presented in Fig. 1. This methodology is devoted to deal with soil-structure interaction elastodynamic problems and it consists of two general steps. First of all, the displacements at soil-structure interface Γ_Ω for a structure Ω_s embedded inside the medium Ω are calculated using a mesh-based method. Numerical approaches such as FEM-BEM and FEM-PML methods are suitable of this task. In step two, the MFS is applied in order to compute the displacement and traction fields on the soil. The displacements on the boundary Γ_Ω obtained in the first step are used as the input boundary conditions for the MFS: the boundary nodes of the mesh-based approach where the boundary condition is evaluated are transformed to collocation points P_c. Virtual sources S_v are located inside the virtual boundary $\tilde{\Gamma}_\Omega$ (which is in geometrical accordance to Γ_Ω), outside the Ω domain, and their strengths are obtained using the fundamental solutions or the Green's function of the soil, depending on whether a full-space or a half-space model of the soil is considered, respectively. In this method, the MFS is proposed to be applied considering the same number of virtual sources than collocation points. Finally, the MFS provides the desired displacement and traction fields on the soil.

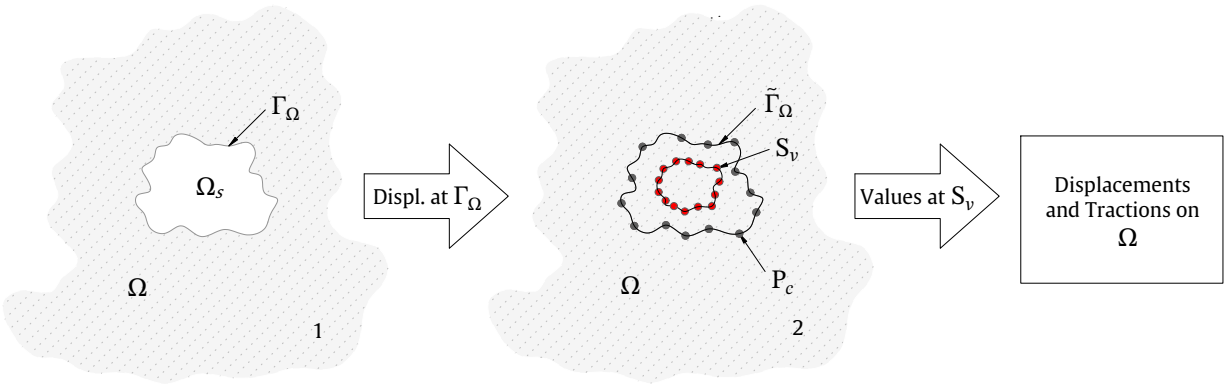

Figure 1: General description of the methodology.

In the current study, this methodology is described for the particular case of longitudinally invariant soil-structure problems, as shown in Fig. 2. To do so, all methods included in the methodology are formulated in the wavenumber-frequency domain (2.5D). Thus, the mesh-based method used to obtain the displacement response at the soil/structure interaction boundary is based on a 2.5D FEM-BEM approach, which is detailed in Section 2.1. The 2.5D MFS approach for elastodynamics used for the computation of the response on the soil domain is presented in Section 2.2. The combination of these two approaches results in a global methodology called 2.5D FEM-BEM-MFS.

Although the method can be potentially applied to problems with arbitrary soil-structure interface geometries, the applications appearing on this paper are restricted to circular boundaries, as also shown in Fig. 2. In this context, collocation points and virtual sources are located along two circumferences of radius R_c and R_s, respectively, with the same angular positions in both cases.

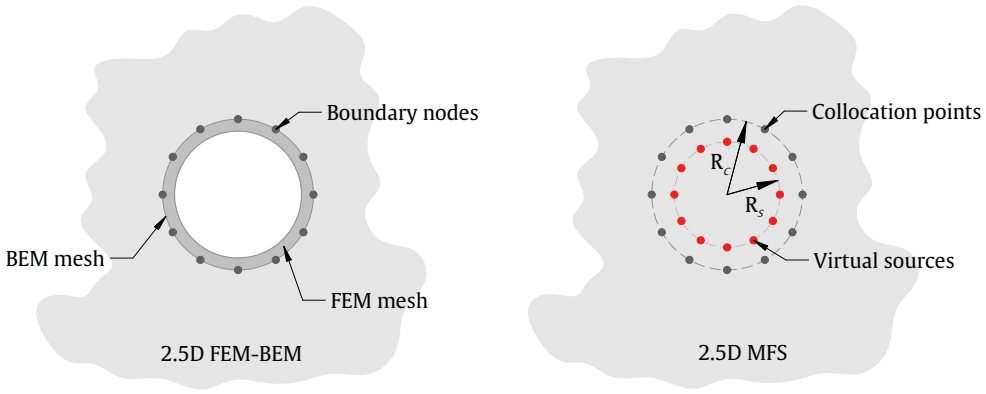

Figure 2: Visual description of the 2.5D FEM-BEM and the 2.5D MFS methods used in this work.

In this work, matrices and tensors are denoted by upper case upright bold letters and vectors are denoted by upper case bold italic letters. Also, the bar notation represents variables in the wavenumber-frequency domain.

2.1. 2.5D FEM-BEM approach

In order to obtain the response at Γ_Ω using a 2.5D FEM-BEM approach, the soil-structure system is divided into two sub-domains, as shown in Fig. 2 (left) for the case of a tunnel structure. The first one consisting of structure and the second one consisting of the unbounded semi-infinite medium, as a model of the soil. The FEM is used to model the first sub-domain relating to the structure and the BEM is used to model the soil. The considered formulation for the 2.5D FEM-BEM approach used in this paper comes from [9], for half-space models of the soil, and from the work of Ghangale et al. [11], for full-space cases. These approaches are chosen for their computational efficiency, particularly significant in the case of [11], and because of the avoidance of using an explicit evaluation scheme of the required singular traction integrals and their capability of using half-space Green's functions, which simplifies the meshing effort. In both methods, the response of the soil-structure system can be obtained by

$$\left[\mathbf{K}_0 - \mathrm{i}k_x\mathbf{K}_1 + k_x^2\mathbf{K}_2 + \bar{\mathbf{K}}_s - \omega^2\mathbf{M}\right]\bar{\boldsymbol{U}} = \bar{\boldsymbol{F}}, \tag{1}$$

where $\mathbf{K}_0$, $\mathbf{K}_1$, $\mathbf{K}_2$ and $\mathbf{M}$ are the stiffness and mass matrices associated to the 2.5D FEM domain, $\bar{\mathbf{K}}_s$ is the dynamic stiffness matrix of the soil obtained from the 2.5D BEM model, k_x is the longitudinal wavenumber, ω is the angular frequency. The stiffness of the soil is frequency and wavenumber dependent, while the stiffness and mass matrices related to FEM domain are independent of them. Moreover, $\bar{\boldsymbol{U}}$ and $\bar{\boldsymbol{F}}$ are the vectors of displacements and applied external forces along the mesh of the structure, respectively. The dynamic stiffness matrix of the soil can be computed by

$$\bar{\mathbf{K}}_s = \boldsymbol{\Phi}\bar{\mathbf{H}}_{bb}^{-1}[\bar{\mathbf{H}}_{bb}^{\tau} + \mathbf{I}], \tag{2}$$

where $\bar{\mathbf{H}}_{bb}$ and $\bar{\mathbf{H}}_{bb}^{\tau}$ are matrices related to the displacement and traction Green's functions, respectively, that relates the response on the boundary due to forces on it. Furthermore, $\mathbf{I}$ represents the identity matrix and $\boldsymbol{\Phi}$ is the transformation matrix that converts the unknown nodal tractions on the boundary to nodal forces.

The response of the soil in terms of displacements, represented by $\bar{\boldsymbol{U}}_f$, can be then obtained by

$$\bar{\boldsymbol{U}}_f = \bar{\mathbf{H}}_{fb}\bar{\boldsymbol{T}}_b - \bar{\mathbf{H}}_{fb}^{\tau}\bar{\boldsymbol{U}}_b, \tag{3}$$

where $\bar{\boldsymbol{U}}_b$ and $\bar{\boldsymbol{T}}_b$ are the vectors of displacements and tractions on Γ_Ω, respectively, and $\bar{\mathbf{H}}_{fb}$ and $\bar{\mathbf{H}}_{fb}^{\tau}$ are the matrices of displacement and traction Green's functions on the medium due to forces on the boundary, respectively. Eq. (3) represents the discretised form of the boundary integral equation in BEM [9]. The displacements on the boundary can be computed using Eq. (1).

Most of the computational time required in this 2.5D FEM-BEM approach relies on the computation of the displacement and traction Green's functions required to construct the matrices $\bar{\mathbf{H}}_{bb}$, $\bar{\mathbf{H}}^{\tau}_{bb}$, $\bar{\mathbf{H}}_{fb}$ and $\bar{\mathbf{H}}^{\tau}_{fb}$, especially for half-space cases, where the Green's functions are not analytical expressions. For full-space cases, strategies to reduce the computational time associated to these matrices are explained in [11]. These strategies can not be directly used in the half-space problems, since the Green's function are also depending on the source depth in comparison with full-space cases, where the only geometric information required from the source and the receiver is its relative distance. For half-space models of the soil, François et al. [9] proposed to obtain these matrices by interpolation over a 2D grid of fixed points. However, using a 2D fixed grid to account for the particular boundary of the problem could result on a significant amount of unnecessary evaluation points. Also, interpolation could result in a loss of accuracy of the system response due to improper sampling of source and evaluation locations. In the present methodology, however, it is proposed to construct a unique set of source-receiver combinations taking into account the relative source-receiver distance and also the source depth. The results on this unique set of source-receiver combinations are then mapped for the original configuration of source and receivers. Refer to [11] for more details on how to construct this unique set of source-receiver combinations and its mapping to the global set. Since for half-space cases this strategy is less efficient than in full-space ones due to the dependency on the source depth, it can be combined with one-dimensional interpolation along the boundary. All this strategy is found to be considerably more efficient in terms of computational time. In the present scheme, the Green's function for 2.5D elastodynamic problems in a full-space are proposed to be obtained with the formulation presented by [30] and adapted by [12], while the Green's functions for homogeneous and layered half-space problems are proposed to be computed using the EDT toolbox [26] or the method proposed by Noori et al. [25], respectively.

2.2. 2.5D MFS approach

The MFS is a mesh-free and integration-free approach for the solutions of the boundary value problems. In this method, a set of virtual sources located outside of the domain which represents the response at the boundary are used to obtain an approximation to the response inside the domain, always by means of the fundamental solutions (or the Green's functions, depending on the problem) of the medium. In the present method, the displacements on the collocation points are obtained from the 2.5D FEM-BEM by computing the response on the boundary. The sources, as shown in Fig. 2 (right), are located outside the domain, i.e. outside the BEM domain from the 2.5D FEM-BEM approach. The displacement and traction Green's functions used in this method are the same ones that are proposed for the 2.5D FEM-BEM approach. Given the displacements at the collocation points, the strengths of the unknowns are calculated as

$$\bar{\boldsymbol{S}}_v = \bar{\mathbf{H}}^{-1}_{cs}\bar{\boldsymbol{U}}_c, \tag{4}$$

where $\bar{\boldsymbol{S}}_v$ is the vector of virtual source strengths, $\bar{\mathbf{H}}_{cs}$ represents the matrix of displacement Green's functions on the collocation points due to the virtual sources and $\bar{\boldsymbol{U}}_c$ represents the displacements at the collocation points. If the collocation points are considered to be directly the nodes of boundary mesh, $\bar{\boldsymbol{U}}_c = \bar{\boldsymbol{U}}_b$. If the configuration is different, the displacement in the collocation points $\bar{\boldsymbol{U}}_c$ should be obtained by interpolation along the boundary from $\bar{\boldsymbol{U}}_b$. Once the source strengths are computed, the displacement and traction responses on the medium, $\bar{\boldsymbol{U}}_f$ and $\bar{\boldsymbol{T}}_f$, can be computed by means of

$$\bar{\boldsymbol{U}}_f = \bar{\mathbf{H}}_{fs}\bar{\boldsymbol{S}}_v, \quad \bar{\boldsymbol{T}}_f = \bar{\mathbf{H}}^{\tau}_{fs}\bar{\boldsymbol{S}}_v, \tag{5}$$

where $\bar{\mathbf{H}}_{fs}$ and $\bar{\mathbf{H}}^{\tau}_{fs}$ represent the source-evaluation points Green's functions for displacements and tractions, respectively, and $\bar{\boldsymbol{U}}_f$ and $\bar{\boldsymbol{T}}_f$ stands for the displacement and traction of the field points, inside the domain.

3. Verification for the case of a structure embedded in a homogeneous full-space

In this section, the current methodology is verified for the case of structures embedded in homogeneous full-spaces. For this verification, two calculation examples are considered: a solid cylinder and a thin circular shell, both embedded

in a homogeneous full-space. The shell has a thickness of 0.1 m and the external radius for both cases is equal to 1 m. The geometrical description of these two case studies can be found in Figs. 3 and 9, respectively. In the example of the solid cylinder, the structure is assumed to be defined by the exact same mechanical parameters than the soil. Thus, for this case, the new methodology results can be compared with the ones obtained with the analytical solution for the 2.5D Green's functions in a homogeneous full-space [30]. Also, the results obtained using a 2.5D FEM-BEM approach [9] of the entire soil-structure system are included in the comparison only for the case of displacement Green's functions. In the case of the thin circular shell, the verification of the new methodology is made only comparing the results with a 2.5D FEM-BEM model of the entire soil-structure system. The mechanical parameters of the soil and the structures appearing in these two examples are presented in Table 1. The FEM meshes of all the structures considered in this verification are done with linear triangular elements. For the solid cylinder, the density of the FEM mesh close to the boundary is selected to have at least 10 boundary elements (BE) per wavelength of the shear waves in the soil and assuming maximum frequencies of 100 Hz and 250 Hz, achieving BEM meshes of 36 and 104 BE, respectively. These two frequencies are selected in accordance to the frequency ranges of interest for ground-borne vibration and noise defined in the standards, which are 1-80 Hz and 16-250 Hz, respectively [20]. For the thin circular shell, meshes for 6 and 10 elements per wavelength are constructed, resulting in 24 and 36 BE, respectively (for a maximum frequency of 100 Hz), and 64 and 104, respectively (for a maximum frequency of 250 Hz). In both calculation cases, the MFS is applied considering the same number of virtual sources than collocation points and a distance between them, defined by $d = R_c - R_s$, of 0.15 m. This value comes from the control scheme presented in Section 5. This verification is shown in terms of two different results: displacement and traction Green's functions in the wavenumber-frequency domain due to a vertical load, presented in dB based on references of 10^{-12} m/(N/m) and 1 (N/m^2)/(N/m), respectively; and also in terms of the receptances and the traction transfer functions obtained from those Green's functions, considering the evaluation point at the longitudinal position x_0 and the longitudinal distribution of the load as $\delta(x-x_0)$, presented in dB based on references of 10^{-12} m/N and 1 (N/m^2)/N, respectively. For this case, the application of the corresponding inverse Fourier transform to compute the receptances and traction transfer functions on the field points from the previously obtained 2.5D Green's functions, can be reduced to the following expressions

$$\boldsymbol{U}_f = \frac{1}{\pi}\int_0^{+\infty} \bar{\boldsymbol{U}}_f \, \mathrm{d}k_x, \qquad \boldsymbol{T}_f = \frac{1}{\pi}\int_0^{+\infty} \bar{\boldsymbol{T}}_f \, \mathrm{d}k_x, \tag{6}$$

where $\boldsymbol{U}_f$ and $\boldsymbol{T}_f$ represent the receptance and the traction transfer function, respectively, at $x = x_0$ due to a force at the same longitudinal location. The previous integration is numerically estimated using a trapezoidal rule with a logarithmic sampling from 0 rad/m to 55 rad/m with 1025 points.

System	Young's modulus [MPa]	Density [kg/m^3]	Poisson's ratio	Damping
Soil	108	1800	0.33	0.05
Solid cylinder	108	1800	0.33	0.05
Thin circular shell	31000	2500	0.2	0.001

Table 1: The characteristics of the problem for full-space and half-space cases

3.1. Solid cylinder embedded in a full-space

In first instance, the verification study for the proposed 2.5D FEM-BEM-MFS method in the case of the solid cylinder is performed based on the displacement Green's functions results. The geometry of the structure, the location of the evaluation points A and B and the location of the force are indicated in Fig. 3. In this case, the mesh of system has a total number of 457 FEM nodes and 36 BEM nodes. The FEM mesh close to the load position is refined to approximately simulate the load considered in the analytical solution, defined in the y-z plane as $\delta(y)\delta(z)$. Points A and B are selected to represent near and far field responses on the soil with respect to the structure, respectively. The comparisons between the different methods are presented in two forms: displacement Green's function plotted against frequency for two fixed wavenumbers, presented in Fig. 4 and plotted against wavenumber for two fixed frequencies, illustrated in Fig. 5. The chosen fixed wavenumbers in Fig. 4 are 0.1 rad/m and 1 rad/m and the fixed

frequencies considered in Fig. 5 are 10 Hz and 50 Hz. As can be seen, very good agreement of the results between the three methods compared is observed in all the plots. The 2.5D FEM-BEM and the analytical solution are matching perfectly in all cases, as expected due to the selection of 10 BE per wavelength. Only slight differences between the 2.5D FEM-BEM-MFS and the other two methods are observed in displacement Green's functions at near field evaluation point (point A) for frequencies higher than 80 Hz, mostly for the wavenumber of 0.1 rad/m.

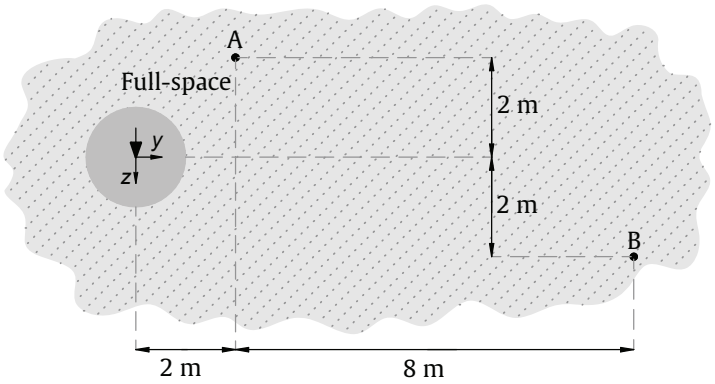

Figure 3: Geometry of the calculation example of a solid cylinder embedded in a full-space. Two evaluation points are considered: A and B. The input vertical force is represented by a big arrow.

Using the same model presented for the displacement Green's functions comparison, the traction Green's functions are compared with the analytical solution of the problem. It can be found that the proposed 2.5D FEM-BEM-MFS approach reaches high levels of accuracy associated to the traction Green's functions in the soil. Again, results at frequencies higher than 80 Hz are the only ones having slight disagreement with respect to the analytical solution. In the case of tractions, these inaccuracies can also be seen in the far field evaluation point, mostly in the case of the wavenumber 0.1 rad/m.

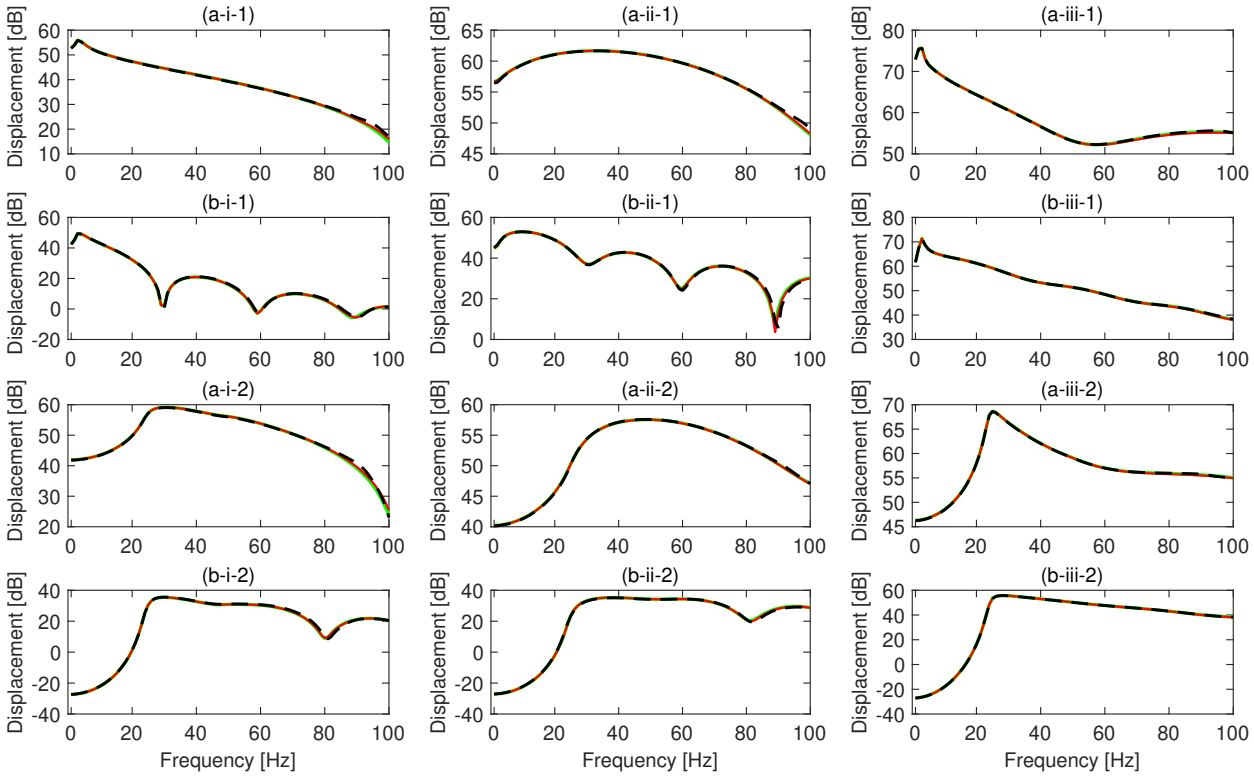

Figure 4: Displacement Green's functions. Methods: 2.5D FEM-BEM (solid red line), 2.5D FEM-BEM-MFS (dashed black line) and analytical solution (solid green line). The results are obtained at points A (a) and B (b) for x (i), y (ii) and z (iii) directions and for wavenumbers of 0.1 rad/m (1) and 1 rad/m (2).

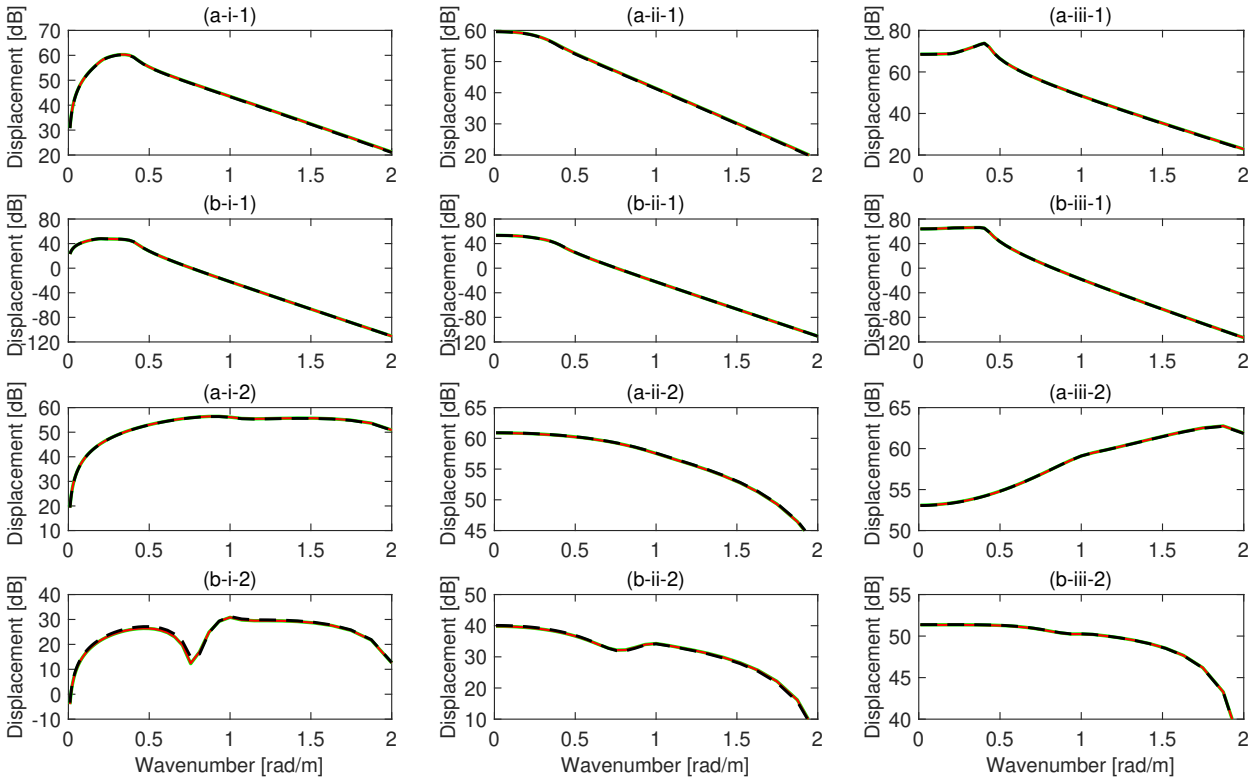

Figure 5: Displacement Green's functions. Methods: 2.5D FEM-BEM (solid red line), 2.5D FEM-BEM-MFS (dashed black line) and analytical solution (solid green line). The results are obtained at points A (a) and B (b) for x (i), y (ii) and z (iii) directions and for frequencies of 10 Hz (1) and 50 Hz (2).

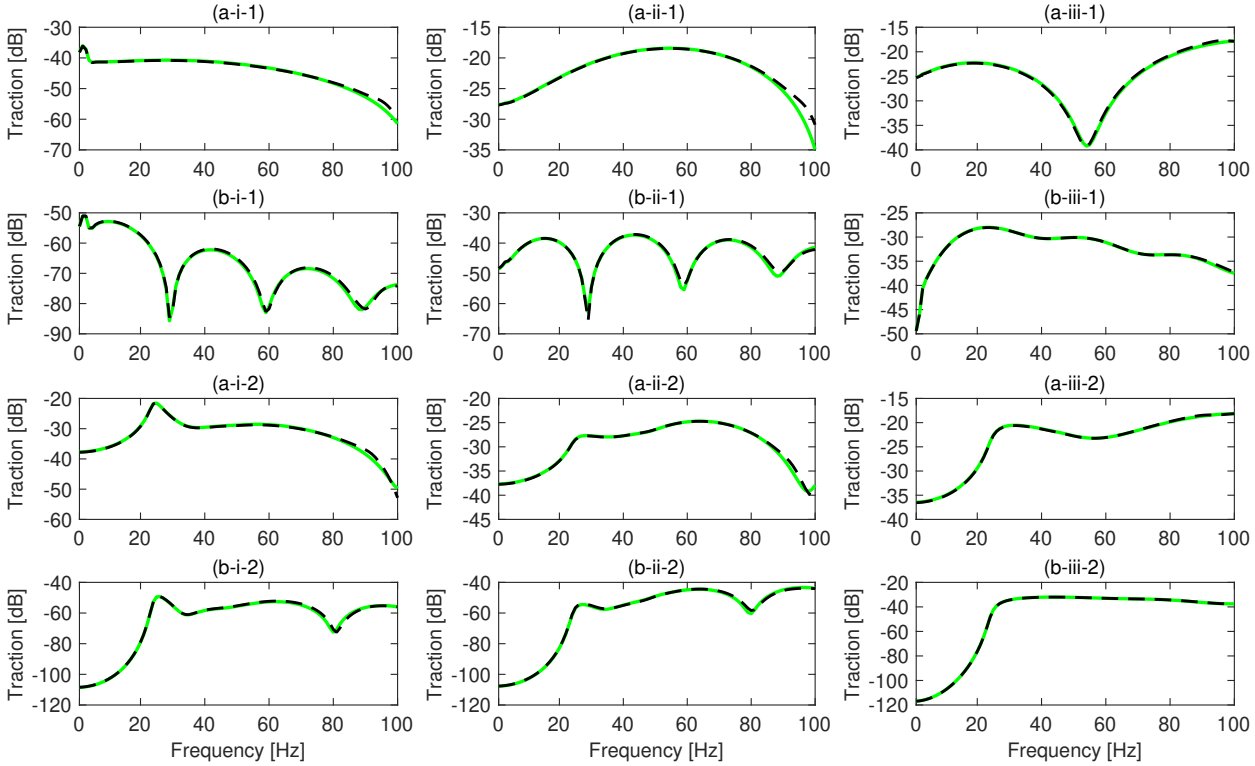

Figure 6: Traction Green's functions. Methods: 2.5D FEM-BEM-MFS (dashed black line) and analytical solution (solid green line). The results are obtained at points A (a) and B (b) for x (i), y (ii) and z (iii) directions and for wavenumbers of 0.1 rad/m (1) and 1 rad/m (2).

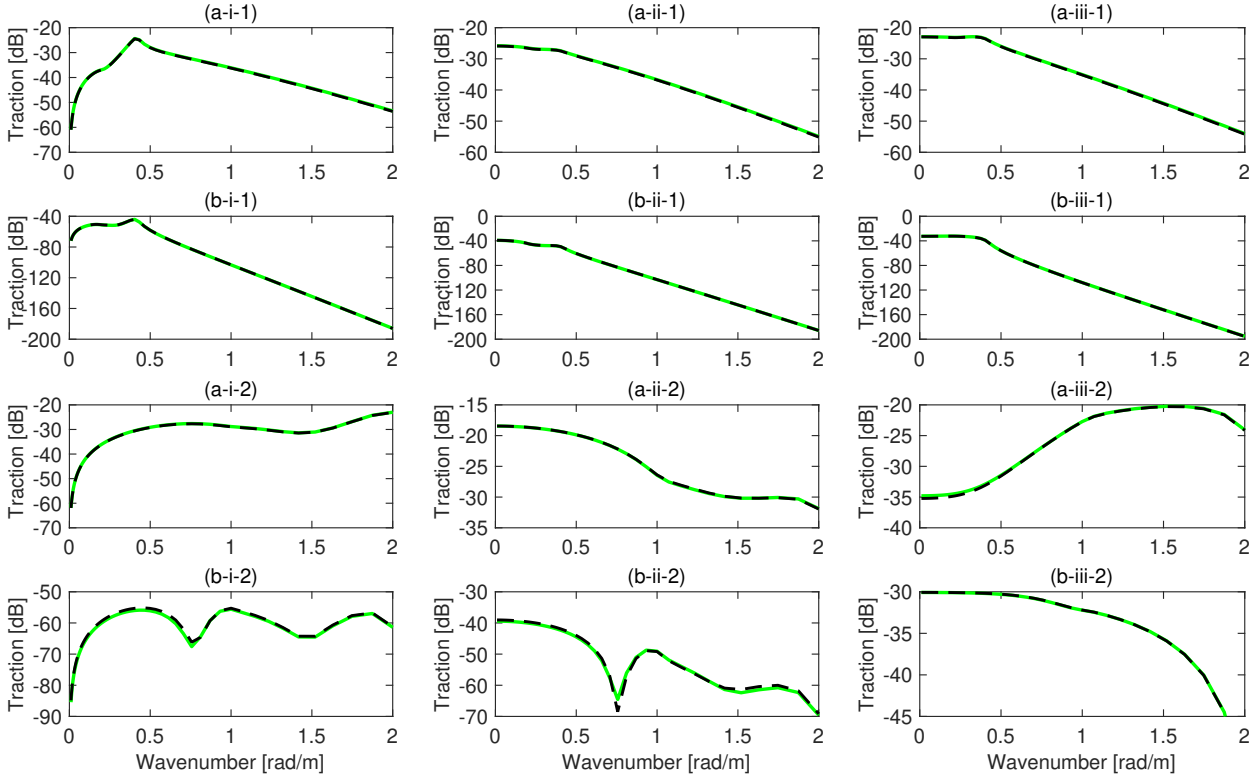

Figure 7: Traction Green's functions. Methods: 2.5D FEM-BEM-MFS (dashed black line) and analytical solution (solid green line). The results are obtained at points A (a), B (b) and C (c) for x (i), y (ii) and z (iii) directions and for frequencies of 10 Hz (1) and 50 Hz (2).

Receptances and traction transfer functions are also considered to verify the method in this case study. In Fig. 8, receptances and traction transfer functions obtained by the proposed methodology are compared with the ones obtained by the 2.5D FEM-BEM approach and the analytical solution of the problem up to 250 Hz. The meshes used here are done imposing 10 BE per wavelength, resulting in a total of 2335 FEM nodes and 104 BEM nodes. In the comparisons presented in this figure related to receptances, only slight discrepancies can be seen between the analytical solution and both numerical methods (which are in full agreement with each other) for frequencies above 200 Hz, for the y component of the response and specially for the near field evaluation point. These discrepancies are also appearing in the case of traction transfer functions.

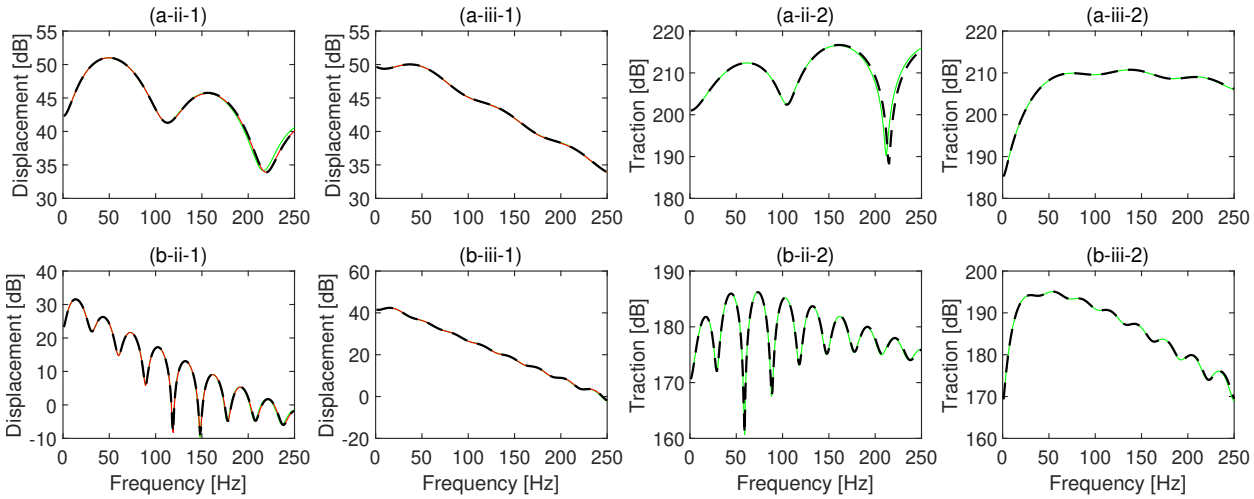

Figure 8: Receptances (1) and traction transfer functions (2). Methods: 2.5D FEM-BEM (solid red line), 2.5D FEM-BEM-MFS (dashed black line) and analytical solution (solid green line). The results are obtained at points A (a) and B (b) for y (ii) and z (iii) directions

.

3.2. Thin circular shell structure embedded in a full-space

As second calculation example, a thin circular shell embedded in a homogeneous full-space is modelled. The geometrical description of the system, the position of the evaluation points considered and the location and direction of the input force are illustrated in Fig. 9. In this example, the new 2.5D FEM-BEM-MFS methodology is compared with a 2.5D FEM-BEM of the entire soil-structure system. In context of these two methods, eight different modelling options are taken into account in the comparison. They are listed and described in Table 2.

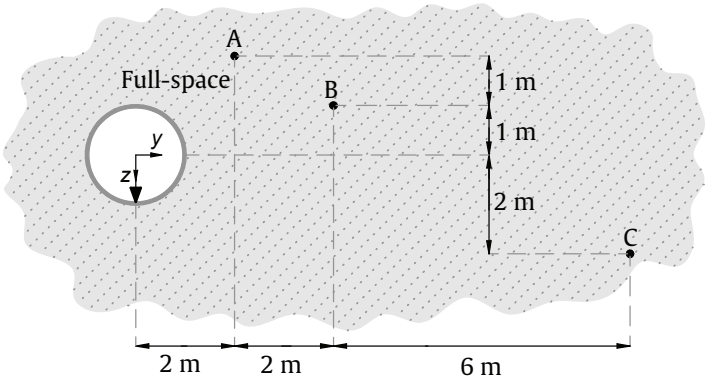

Figure 9: Geometry of the calculation example of a thin circular shell structure embedded in a full-space. Three evaluation points are considered: A, B and C. The input vertical force is represented by a big arrow.

In this example, the comparison is done in terms of the receptances due to a vertical force applied in the bottom of the cavity. For the calculation of the receptances, the wavenumber in the x direction was logarithmically sampled from 0 rad/m to 55 rad/m with 1025 points. In first instance, modelling options associated to maximum frequency of 100 Hz are compared. For this case, the differences between the five proposed numerical models are negligible for frequencies below 80 Hz. Thus, receptances are plotted in Fig. 10 only in the frequency range from 80 Hz to 100 Hz, where the most significant discrepancies between methods can be seen. From the observation of these plots, the first insight that arises is that 2.5D FEM-BEM and 2.5D FEM-BEM-MFS methods show a strong agreement when the number of boundary nodes considered is the same, which verifies the new proposed approach for the present calculation

Max. frequency	BE per λ_s	Modelling options	$N_{\text{BEM}}/N_{\text{CP}}$	N_{FEM}
100 Hz	6	2.5D FEM-BEM-24	24	241
		2.5D FEM-BEM-MFS-24-24	24/24	241
		2.5D FEM-BEM-MFS-24-36	24/36	241
	10	2.5D FEM-BEM-36	36	283
		2.5D FEM-BEM-MFS-36-36	36/36	283
250 Hz	6	2.5D FEM-BEM-MFS-64-64	64/64	563
	10	2.5D FEM-BEM-MFS-104	104	603
		2.5D FEM-BEM-MFS-104-104	104/104	603

Table 2: Specifications of the modelling options considered for the case of thin shell structure. In this table, λ_s represents the wavelength for the maximum frequency and N_{BEM}, N_{FEM} and N_{CP} represent the number of BEM nodes, FEM nodes and collocation points, respectively.

example. The modelling option 2.5D FEM-BEM-MFS-24-36 is an enhanced version of the 2.5D FEM-BEM-MFS-24-24 one, where the displacements on the 24 boundary nodes are interpolated based on a third degree polynomial to a set of 36 collocation points. As can be observed in Fig. 10, this method generally increases the accuracy of the 2.5D FEM-BEM-MFS when it is compared with a 2.5D FEM-BEM with the same number of boundary nodes, giving improved results with respect to the 2.5D FEM-BEM-MFS-24-24 method. However, it should be noted that the interpolation-based methodology can only converge to the solution for the same number of boundary nodes. Due to that, the accuracy level of the 2.5D FEM-BEM-MFS-24-36 results is similar to the one associated to the 2.5D FEM-BEM-24 method but lower than the 2.5D FEM-BEM-MFS-36-36 one.

Furthermore, the results obtained by the modelling options associated to a maximum frequency of 250 Hz are shown in Fig. 11. The accuracy of the proposed method, even for the 2.5D FEM-BEM-MFS-64-64 model, has been found to be high. The interpolation-based method is not considered in this comparison due to high accuracy of that non-interpolated 2.5D FEM-BEM-MFS-64-64 method.

The computational efficiency of the current method is studied with respect to 2.5D FEM-BEM solution in the context of the thin shell case study with 36 BEM nodes. Both methodologies have been implemented in MATLAB. The efficiency comparison is performed over a high performance cluster with 2 GHz Intel® Xeon® Gold 6138 CPU (with 40 cores). The computational efficiency of the methodology is investigated for two case scenarios. Firstly, a computation for 2048 wavenumber values, a frequency of 50 Hz and only one evaluation point is performed in only one core of the cluster and the computational costs are assessed. The results indicate that the 2.5D FEM-BEM methodology consumes 78 seconds to obtain the displacement response in the evaluation point, while the current methodology spends a total time of 69 seconds, divided in 63 seconds to get the response in the collocation points with the 2.5D FEM-BEM and 6 seconds to obtain the field point response using the 2.5D MFS (the latter computational time includes the source strengths computation). In the second example, the algorithms are run for one value of the wavenumber and the frequency, and for 5, 25, 100, 500, 1000 and 2500 evaluation points. The computational costs of both methods for this second example are indicated in Table 3. It is worth to be mentioned that the computational time to obtain the boundary conditions by 2.5D FEM-BEM in the context of the 2.5D FEM-BEM-MFS method is equal to 0.119 seconds and it is constant for all cases. According to the results, the time consumed by the 2.5D FEM-BEM method increases exponentially with respect to the number of evaluation points, while the computational cost of the current methodology increases in a linear trend also with respect to the number of evaluation points. Thus, the computational efficiency of the current methodology with respect to the 2.5D FEM-BEM method is demonstrated to be very high for large amounts of evaluation points, while the improvement for few evaluation points is almost insignificant.

Number of evaluation points	5	25	100	500	1000	2500
Computational time using 2.5D FEM-BEM-MFS [s]	0.9	0.91	0.96	1.02	1.08	1.32
Computational time using 2.5D FEM-BEM [s]	2.46	2.49	2.82	5.3	11.8	48.1

Table 3: Computational costs of both methods depending of the number of evaluation points considered.

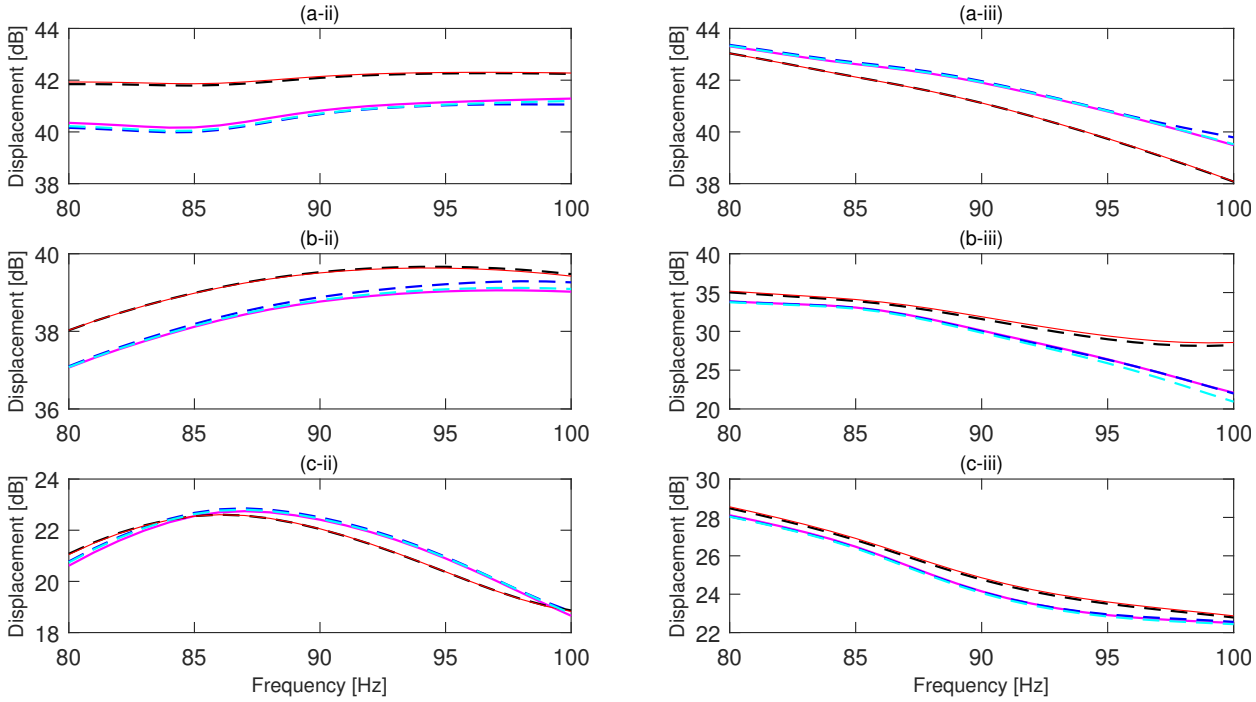

Figure 10: Receptances. Methods: 2.5D FEM-BEM-36 (solid red line), 2.5D FEM-BEM-24 (solid magenta line), 2.5D FEM-BEM-MFS-24-24 (dashed blue line), 2.5D FEM-BEM-MFS-24-36 (dashed cyan line) and 2.5D FEM-BEM-MFS-36-36 (dashed black line). The results are obtained at points A (a), B (b) and C (c) for y (ii) and z (iii) directions.

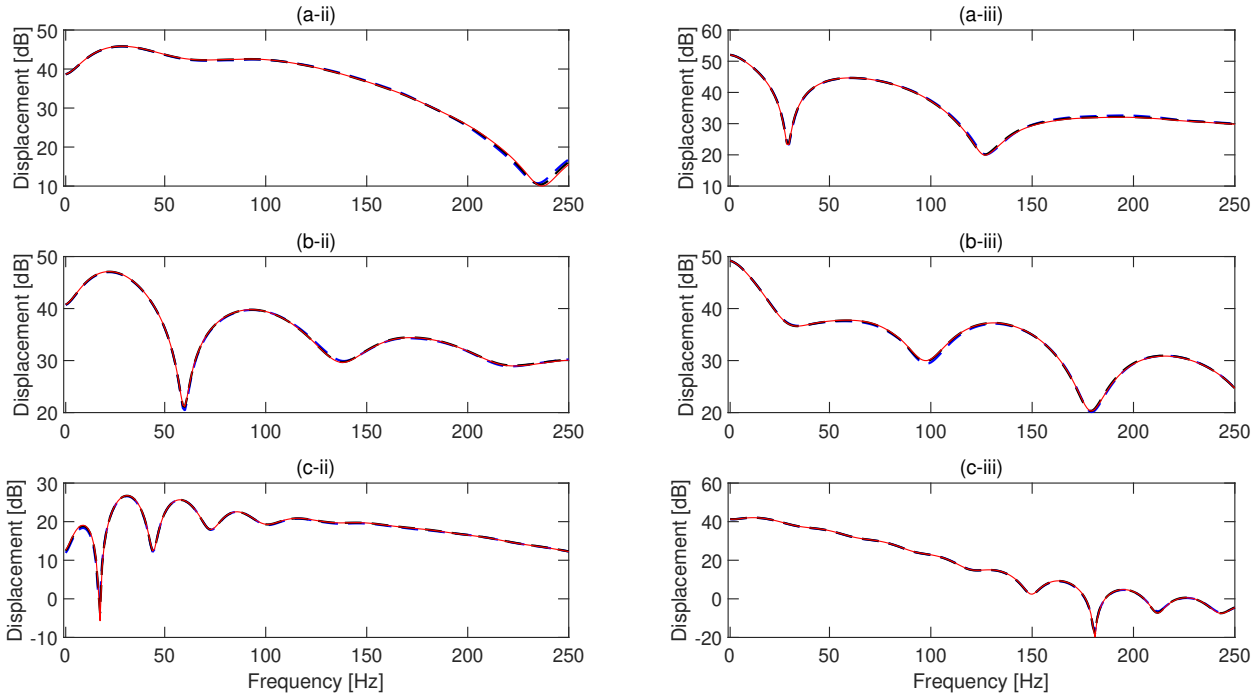

Figure 11: Receptances. Methods: 2.5D FEM-BEM-104 (solid red line), 2.5D FEM-BEM-MFS-64-64 (dashed blue line) and 2.5D FEM-BEM-MFS-104-104 (dashed black line). The results are obtained at points A (a), B (b) and C (c) for y (ii) and z (iii) directions.

4. Verification for the case of a structure embedded in a homogeneous half-space

In this section, the performance of the current method is verified for the case of structures embedded in homogeneous half-spaces. The verification is performed for two examples: a solid cylinder and a thin circular shell, both buried in a homogeneous half-space. The external radius for both structures is equal to 1 m and the shell thickness is equal to 0.1 m. The geometrical characteristics of these two calculation examples are indicated in Figs. 12 and 18, respectively. As assumed in the full-space case, the same material is used for the structure and medium for the solid cylinder case. The material properties are described in Table 1. Therefore, the results of this case can be directly compared with the semi-analytical solution for the 2.5D Green's functions of a homogeneous half-space. The semi-analytical solution is obtained in the basis of the direct stiffness method proposed by Kausel [21] using the EDT toolbox [26]. The 2.5D Green's functions required in 2.5D FEM-BEM-MFS and 2.5D FEM-BEM methods are also computed in this way for both calculation examples. The FEM meshes for these cases are the same ones that have been created for the full-space ones. The MFS is also applied for these calculation examples considering the same number of virtual sources than collocation points and a distance between them of 0.15 m. Results presented in this section are of the same form as the ones presented for the full-space cases.

4.1. Solid cylinder embedded in a half-space

As explained before, three types of results are compared in the verification of the new proposed approach for the displacement Green's functions in the case of the solid cylinder embedded in a half-space: the ones obtained by 2.5D FEM-BEM-MFS, by the 2.5D FEM-BEM and by the semi-analytical solutions of a homogeneous half-space. The geometry of the structure, the location of the evaluation points A, B and C and the location of the force are indicated in Fig. 12. The evaluation point A is located on the ground surface and points B and C are located in the soil to investigate the near and far field responses, respectively. According to Figs. 13 and 14, the Green's function

displacements for all calculation cases are consistent with those obtained by the semi-analytical method and 2.5D FEM-BEM approach. The only significant difference is observed in the displacement in the y component in point B for the wavenumber of 0.1 rad/m (Fig. 13 (b-ii-1)), where errors up to 16% difference at high frequencies (higher than 80 Hz) for both 2.5D FEM-BEM-MFS and 2.5D FEM-BEM approaches with respect to the semi-analytical solution are observed.

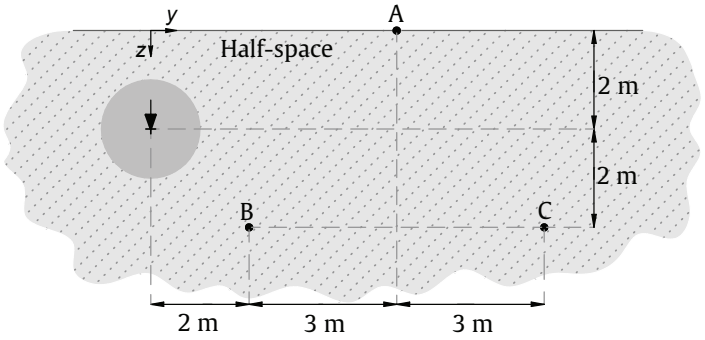

Figure 12: Geometry of the calculation example of a solid cylinder embedded in a half-space. Three evaluation points are considered: A, B and C. The input vertical force is represented by a big arrow.

In the case of traction Green's functions, the verification study only accounts for the 2.5D FEM-BEM-MFS and the 2.5D FEM-BEM methods. The comparison of these two methods for the selected calculation parameters are illustrated in Figs. 15 and 16. As demonstrated in the presented plots, very good accuracy of the traction Green's functions is provided by the new method. Since the traction Green's function in vertical direction are equal to zero for evaluation points at the ground surface, no plot is presented for the z component in the point A. Only slight differences at frequencies higher than 80 Hz can be observed, again, for the y component of the traction in point B the wavenumber of 0.1 rad/m (Fig. 15 (b-ii-1)) and also for the wavenumber of 1 rad/m (Fig. 15 (b-ii-2)).

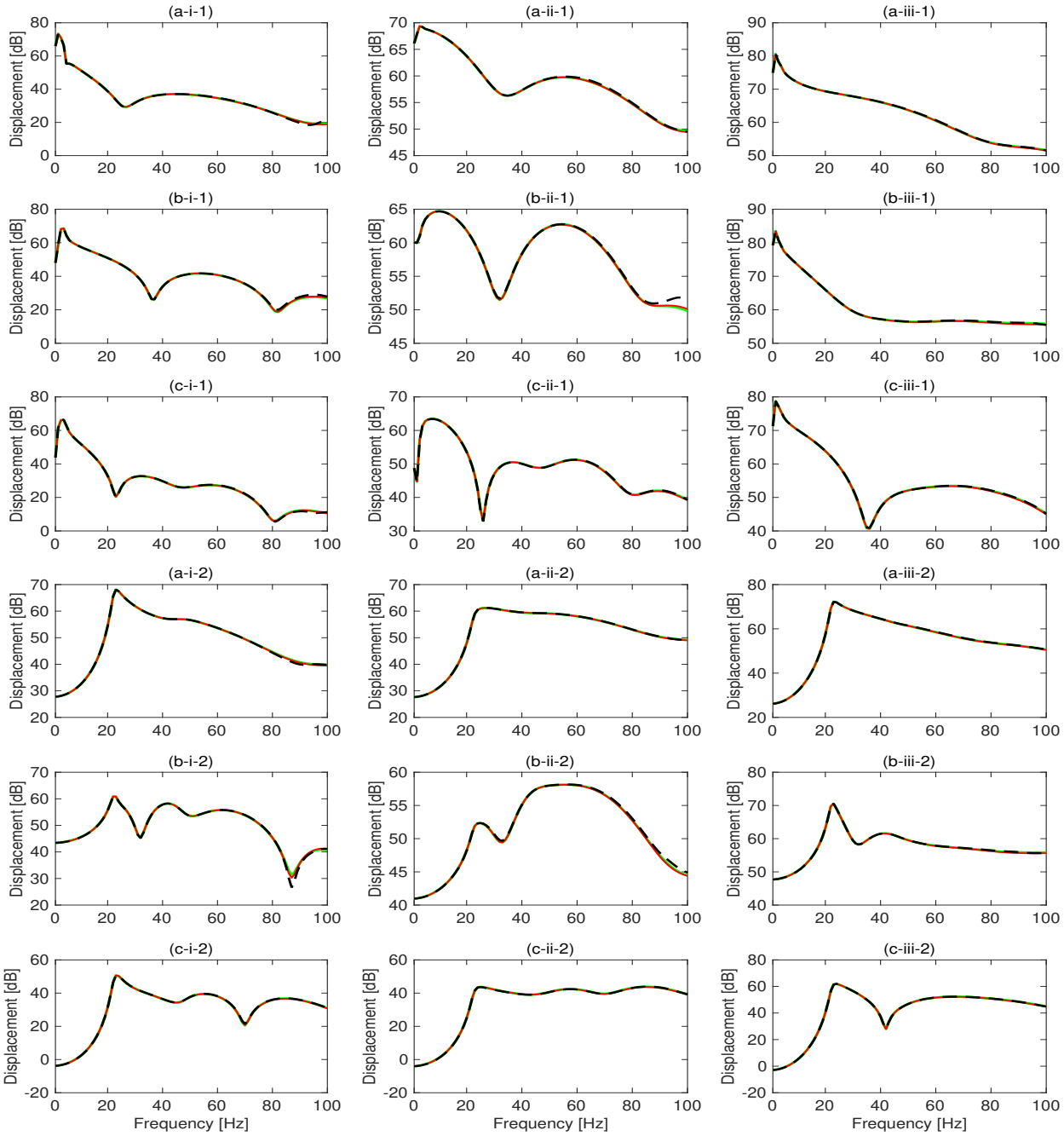

Figure 13: Displacement Green's functions. Methods: 2.5D FEM-BEM (solid red line), 2.5D FEM-BEM-MFS (dashed black line) and semi-analytical solution (solid green line). The results are obtained at points A (a), B (b) and C (c) for x (i), y (ii) and z (iii) directions and for wavenumbers of 0.1 rad/m (1) and 1 rad/m (2).

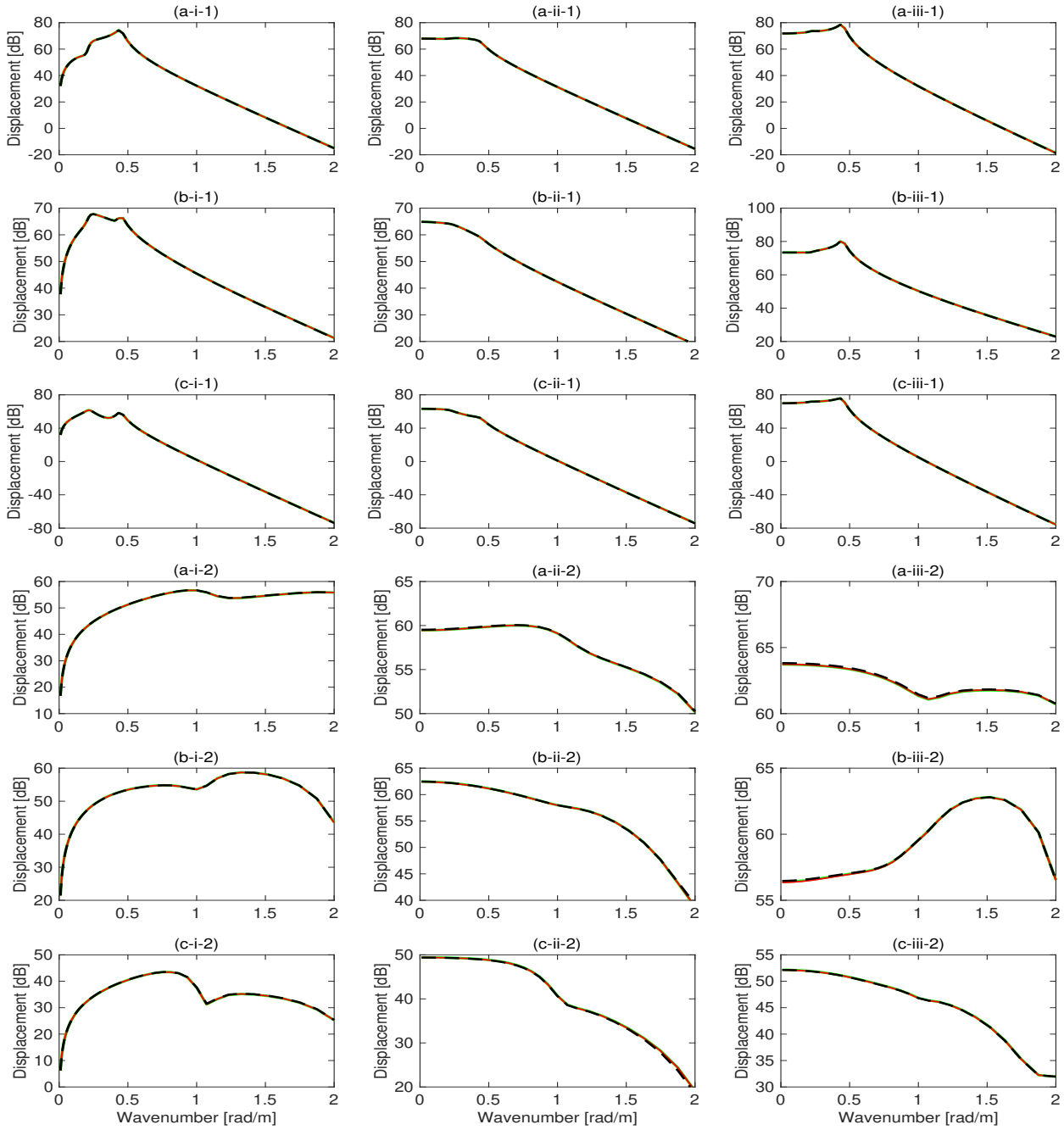

Figure 14: Displacement Green's functions. Methods: 2.5D FEM-BEM (solid red line), 2.5D FEM-BEM-MFS (dashed black line) and semi-analytical solution (solid green line). The results are obtained at points A (a), B (b) and C (c) for x (i), y (ii) and z (iii) directions and for frequencies of 10 Hz (1) and 50 Hz (2).

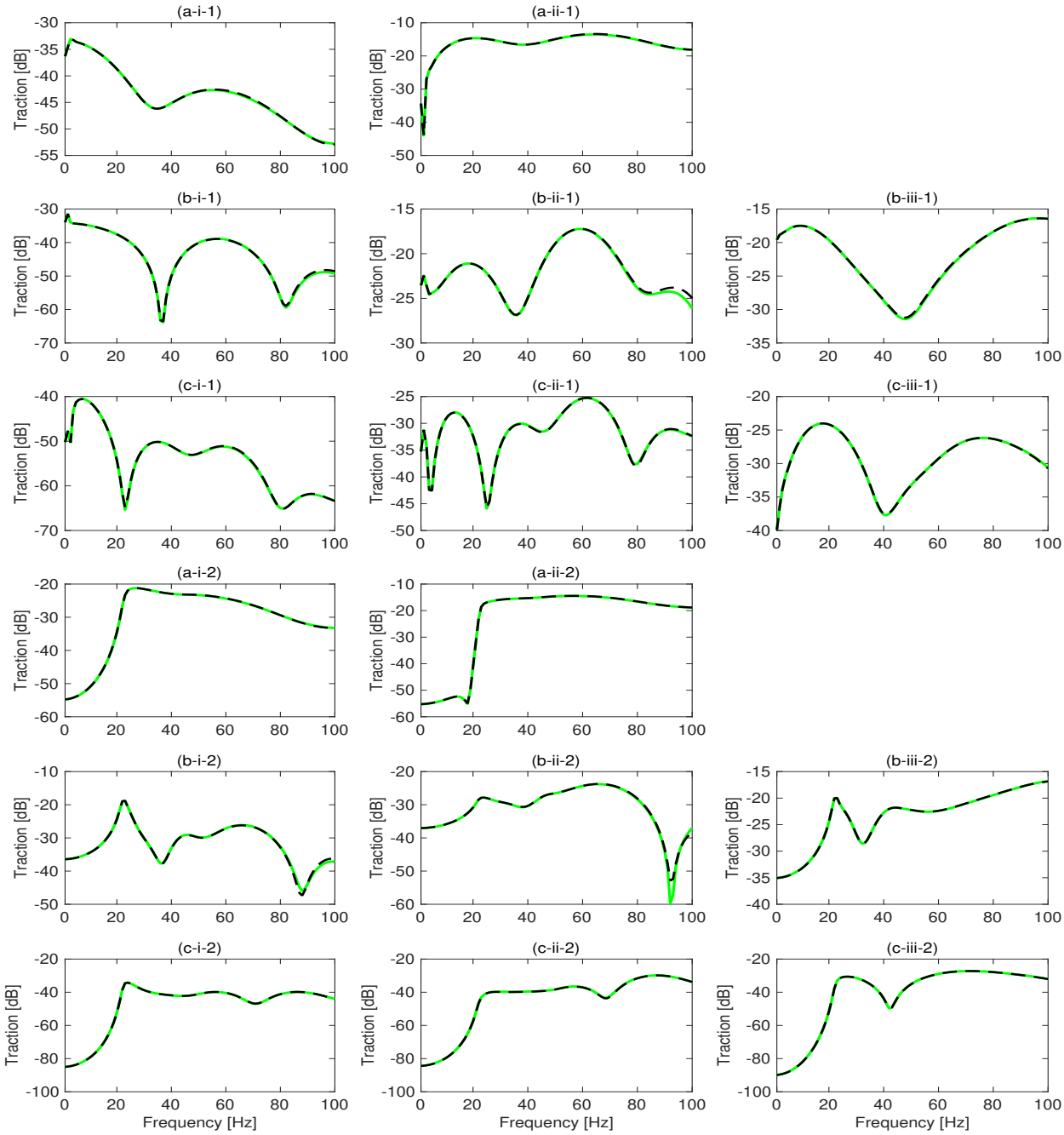

Figure 15: Traction Green's functions. Methods: 2.5D FEM-BEM-MFS (dashed black line) and semi-analytical solution (solid green line). The results are obtained at points A (a), B (b) and C (c) for x (i), y (ii) and z (iii) directions and for wavenumbers of 0.1 rad/m (1) and 1 rad/m (2).

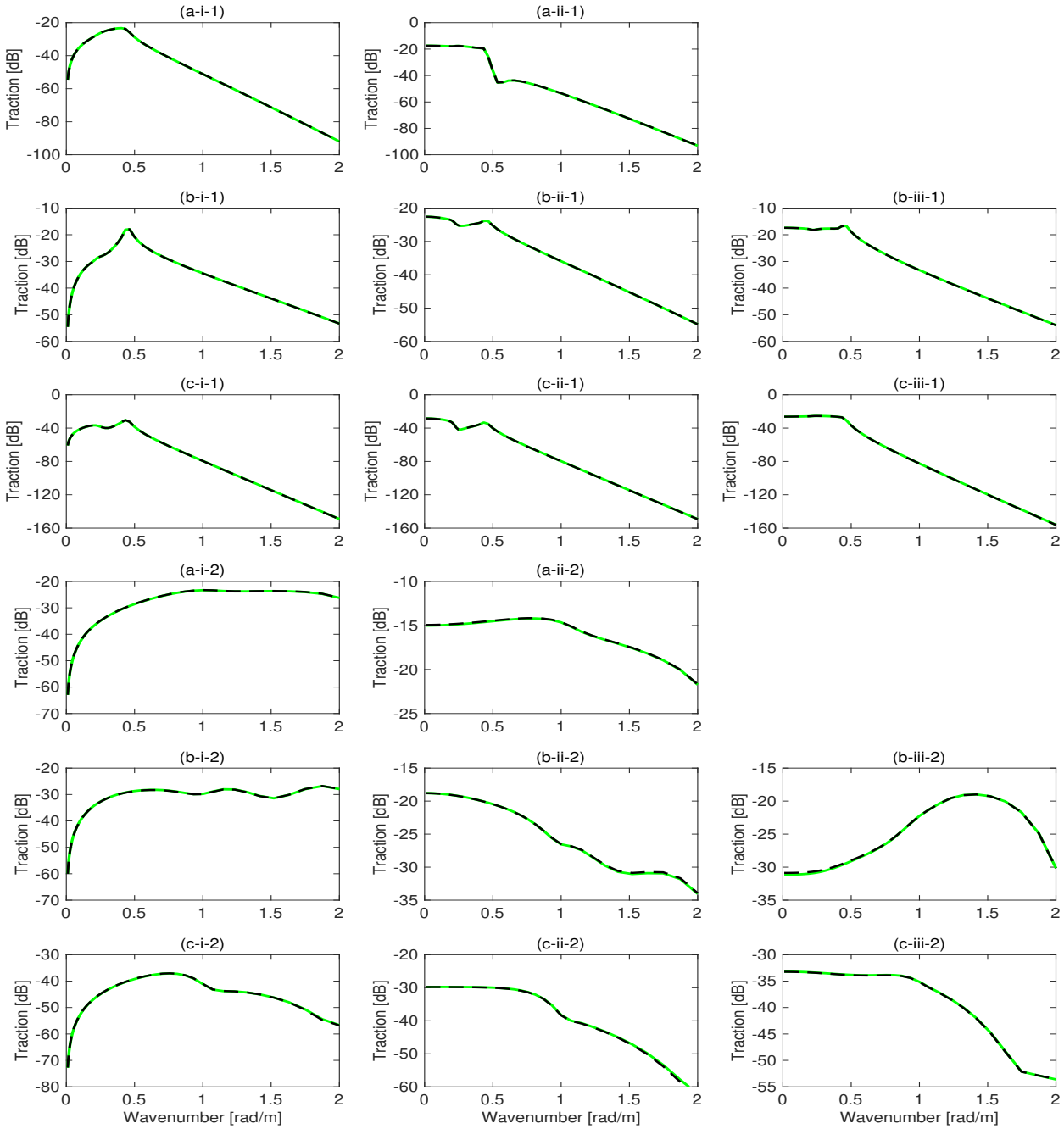

Figure 16: Traction Green's functions. Methods: 2.5D FEM-BEM-MFS (dashed black line) and semi-analytical solution (solid green line). The results are obtained at points A (a), B (b) and C (c) for x (i), y (ii) and z (iii) directions and for frequencies of 10 Hz (1) and 50 Hz (2).

Moreover, the accuracy of the proposed method is also studied in terms of receptances and traction transfer functions. The same mesh with 10 BE per wavelength and a maximum frequency of 250 Hz used in the full-space cases is adopted here. Results of this study are presented in Fig. 17, where the proposed method is compared with the 2.5D FEM-BEM approach and the semi-analytical solution. To compute the desired transfer functions, the wavenumber in the longitudinal direction was logarithmically sampled from 0 rad/m to 55 rad/m with 257 points. Slight discrepancies are observed at frequencies above 200 Hz for the y and z components of the response in the field points B and C, for both receptances and traction transfer functions.

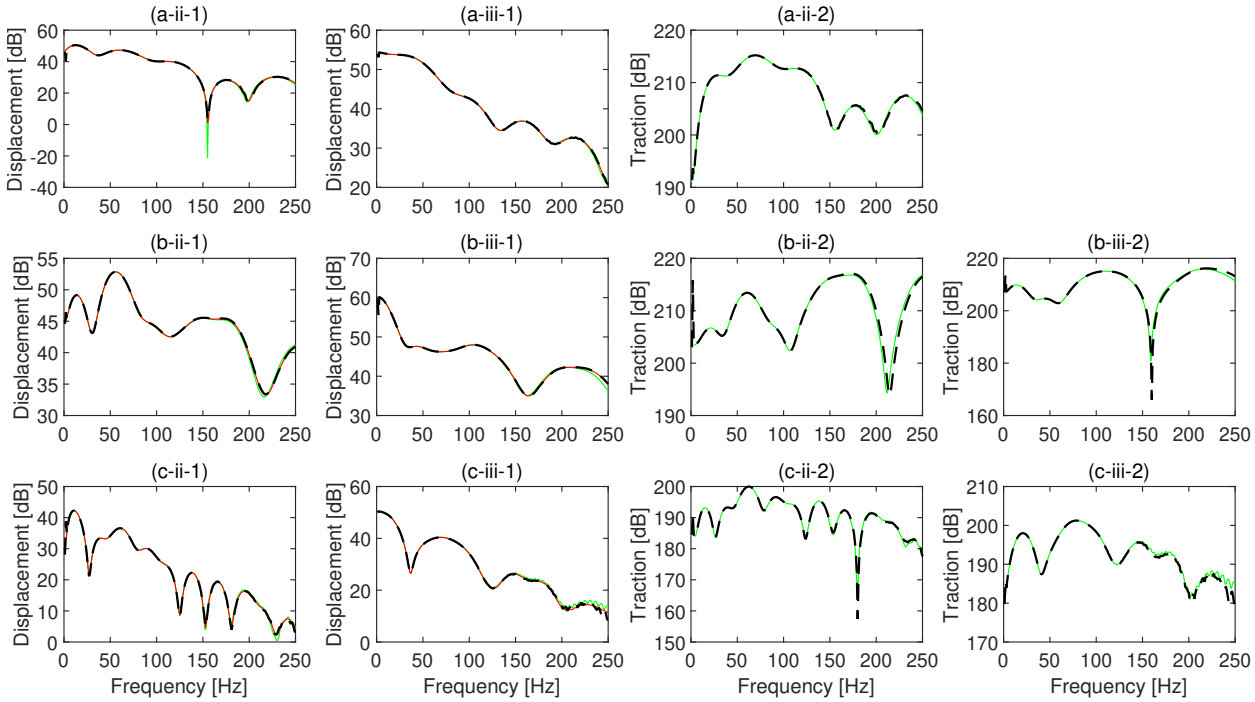

Figure 17: Receptances (1) and traction transfer functions (2). Methods: 2.5D FEM-BEM (solid red line), 2.5D FEM-BEM-MFS (dashed black line) and semi-analytical solution (solid green line). The results are obtained at points A (a), B (b) and C (c) for y (ii) and z (iii) directions

.

4.2. Thin circular shell structure embedded in a half-space

The last case study considered in this work and presented in this section consists of a thin circular shell embedded in a homogeneous half-space. The studied system is visually described in Fig. 18, where the evaluation points and the input force are defined. For this example, the same eight modelling options described in section 3.2 are also taken into consideration here. For the methods comparison, results are shown in terms of the receptances. In this case, the wavenumber in the longitudinal direction was logarithmically sampled from 0 rad/m to 55 rad/m with 129 points. For the case of a maximum frequency of 100 Hz, this comparison is presented in Fig. 19 only for the frequency range of 80 Hz to 100 Hz. As shown for the case of a thin shell embedded in a full-space, significant differences between the different methods compared can only be seen above 80 Hz. Following the same trend than full-space case results, Fig. 19 shows that the receptances obtained by 2.5D FEM-BEM and 2.5D FEM-BEM-MFS methods are approximately matching when the number of boundary nodes is equal, confirming the accuracy of the new method. The interpolation-based method applied in the 2.5D FEM-BEM-MFS-24-36 modelling option is slightly improving the accuracy of the results, as also encountered in the full-space case study. Modelling options associated to a maximum frequency of 250 Hz are compared in Fig. 20. Similarly to the full-space case, very good agreement is observed between three modelling options.

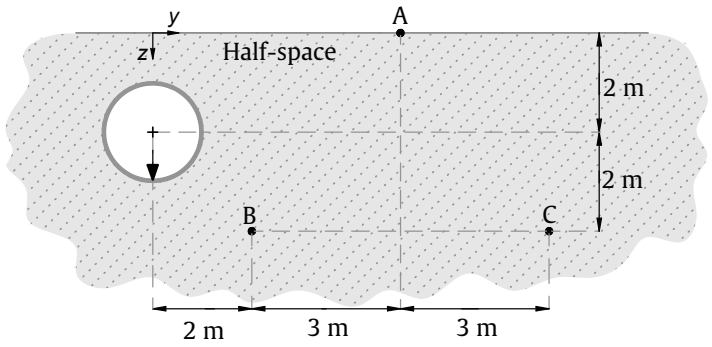

Figure 18: Geometry of the thin circular shell structure studied in this paper for the verification of the 2.5D FEM-BEM-MFS half-space. Three evaluation points are considered: A, B and C. The input vertical force is represented by a big arrow.

The computational efficiency of the current method is compared to the 2.5D FEM-BEM approach in the context of the thin shell case study with 36 BEM nodes. Both methodologies have been implemented in MATLAB and have been executed with the same desktop configuration described in full-space problem. The computational cost of the methods is studied for two different cases. Firstly, the results are compared for one evaluation point, one frequency and 128 wavenumber values. The running times for the new method and for 2.5D FEM-BEM are 702 (divided in 431 seconds for the 2.5D FEM-BEM and 271 seconds for the 2.5D MFS) and 475 seconds, respectively. Due to EDT toolbox algorithm design, the new method is even slower than the 2.5D FEM-BEM; however, it should be noted that the benefits of the method are arisen for large amounts of evaluation points. Secondly, a computational efficiency study is carried out taking one value of the wavenumber and the frequency and 5, 25, 60, 100, 160 and 200 evaluation points. The total computational costs consumed by 2.5D FEM-BEM-MFS and 2.5D FEM-BEM methods are shown in Table 4. It should be noted that the computational time to obtain the boundary conditions in the 2.5D FEM-BEM-MFS by the 2.5D FEM-BEM is equal to 4.5 seconds regardless of the amount of evaluation points. Based on the findings, the computational time spent by both methods raises with a quadratic trend with respect to the number of evaluation points, being the second-order coefficient associated to the curve obtained from the new considerably smaller than the one associated to the 2.5D FEM-BEM approach. Although the computational efficiency of the current methodology for half-space problems has increased, the improvement does not reach the same improvement levels of the method in full-space cases. That is due to the semi-analytical nature of the 2.5D elastodynamic Green's functions of a half-space and also because of the selected algorithm to calculate them, which in this case is the EDT toolbox.

Number of evaluation points	5	25	60	100	160	200
Computational time using 2.5D FEM-BEM-MFS [s]	7.5	10	15	20	30	45
Computational time using 2.5D FEM-BEM [s]	15	20	44	70	181	241

Table 4: Computational costs of both methods depending of the number of evaluation points considered.

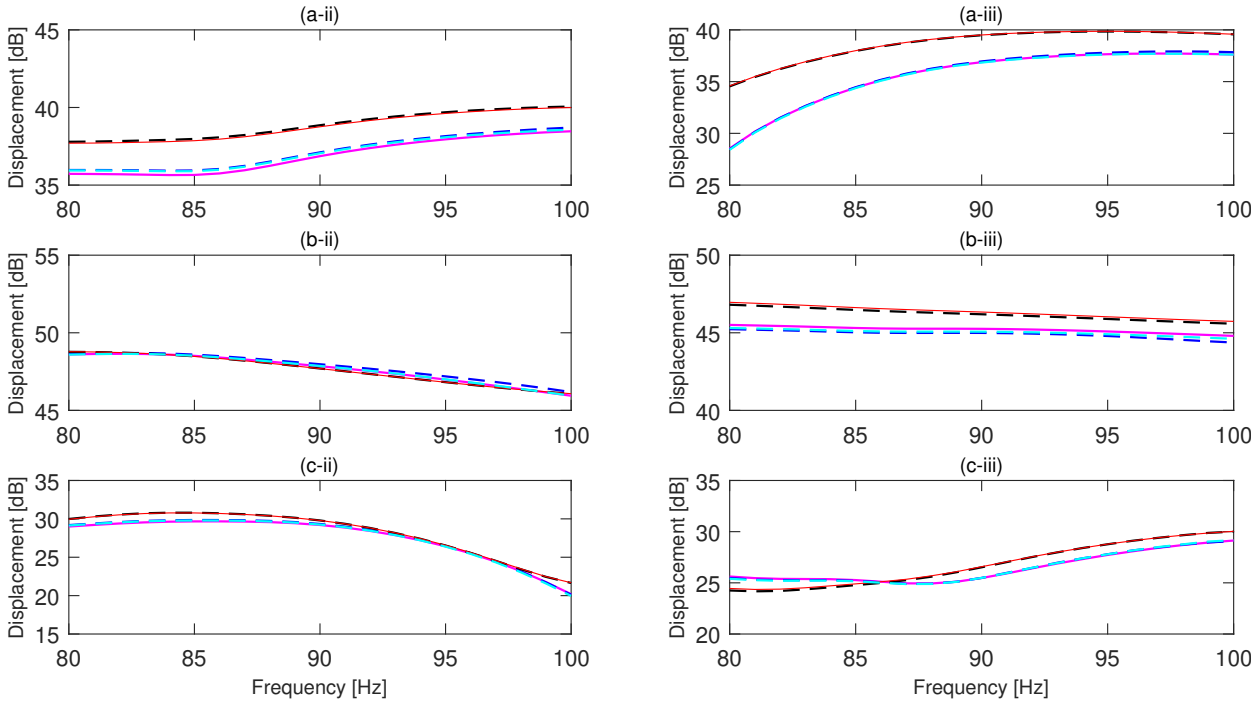

Figure 19: Receptances. Methods: 2.5D FEM-BEM-36 (solid red line), 2.5D FEM-BEM-24 (solid magenta line), 2.5D FEM-BEM-MFS-24-24 (dashed blue line), 2.5D FEM-BEM-MFS-24-36 (dashed cyan line) and 2.5D FEM-BEM-MFS-36-36 (dashed black line). The results are obtained at points A (a), B (b) and C (c) for y (ii) and z (iii) directions.

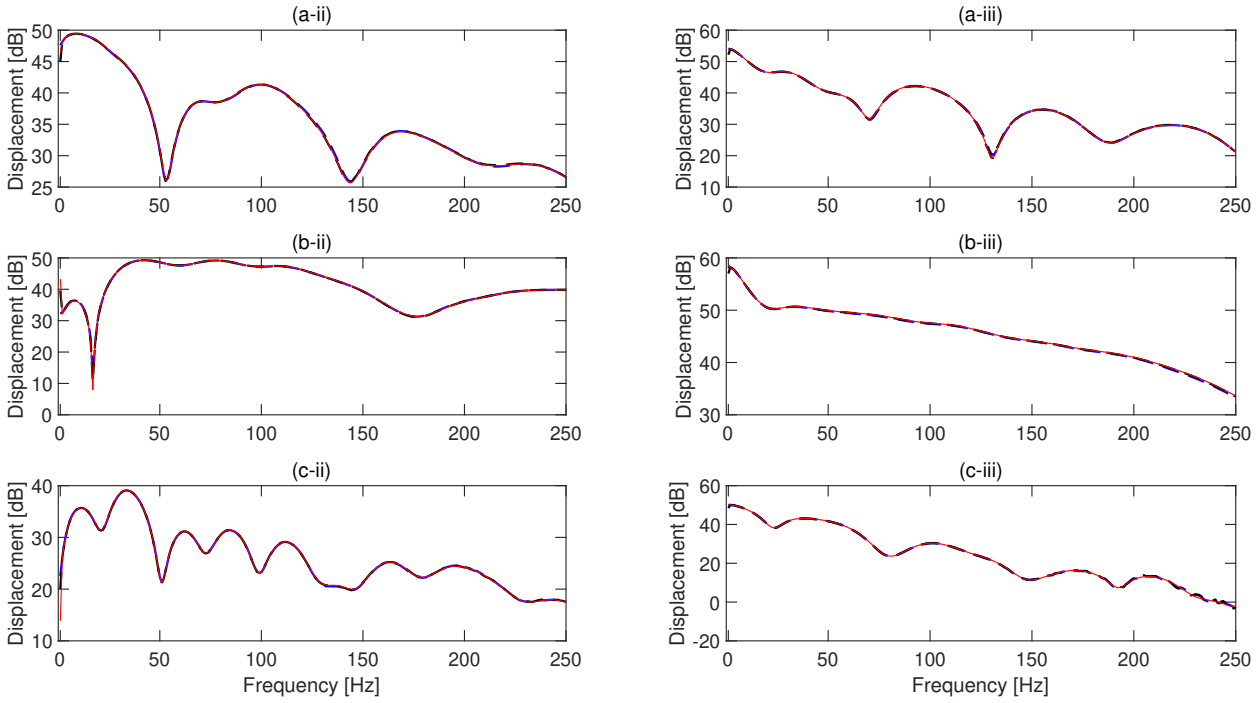

Figure 20: Receptances. Methods: 2.5D FEM-BEM-104 (solid red line), 2.5D FEM-BEM-MFS-64-64 (dashed blue line) and 2.5D FEM-BEM-MFS-104-104 (dashed black line). The results are obtained at points A (a), B (b) and C (c) for y (ii) and z (iii) directions.

5. Control methodology for MFS robustness

As mentioned in the introduction section, the distance between collocation and source points in MFS should be properly selected to avoid large numerical errors of the method. In the present section, a control technique that finds the optimal distance between collocation and source points that minimises the error of the method is described. The error of the method is evaluated in a limited group of points in the medium, called control points, distributed in the area where the final results are required. Assuming a MFS application where the number of virtual forces is always the same than collocation points, as adopted in the present work, the distance between collocation points and virtual sources d is the only variable that should be selected and, thus, the only variable that controls the robustness of the method: This is because the collocation points coincide with the BEM nodes of the BEM mesh, created on the basis of 6-10 BE per wavelength, making the number of virtual sources inherently assigned. In order to optimise d without losing computational efficiency, the control technique is carried out only considering three field points (near, medium and far field locations), three frequencies (representing low, medium and high values of the total frequency range) and two wavenumbers (representing low and high values of the total wavenumber range). The relative error is calculated at these sampling points for various values of the distance d by comparing the results obtained by the 2.5D FEM-BEM-MFS method and those obtained from the 2.5D FEM-BEM approach. From those relative errors, the optimal d is chosen. Consequently, this control method is not affecting the overall computational efficiency of the methodology if the amount of sampling points (considering field points, frequency and wavenumber) are large, which is the common situation for soil-structure interaction problems. Unless to the previous techniques [4, 1], the proposed control method is easier to be implemented. A relative error parameter ε_r is defined to determine the robustness of the method [15].

$$\varepsilon_r = \sqrt{\frac{1}{3N}\sum_{i=1}^{3}\sum_{j=1}^{N}\left|\frac{\bar{U}_{fn}^{ij}-\bar{U}_{fr}^{ij}}{\bar{U}_{fr}^{ij}}\right|^2} \tag{7}$$

where i and j are the indices associated to the three displacement components and the N control points, respectively. Moreover, $\bar{U}_{fn}^{ij}$ and $\bar{U}_{fr}^{ij}$ represent the displacements obtained by the new method and by a reference method, respectively, in the control point j and in the direction i. For all the cases, the reference method is the 2.5D FEM-BEM approach.

In this investigation, this control methodology has been applied to the four calculation examples described in Sections 3 and 4. The control points considered are the evaluation points selected in each case. In Figs. 21 and 22, the relative error in full-space and half-space cases, respectively, is plotted for frequencies ranging 1 Hz to 100 Hz and for distances d ranging between 5 cm to 75 cm and for two wavenumbers: 0.1 rad/m and 1 rad/m. From the optimisation process for the calculation examples in full-space, it can be seen that only distances lower than 0.1 m are not recommended. The rest of the source-collocation points distances in the range considered are resulting in accurate results and very similar to each other. Only some slight errors appear as constant trends with respect to the distance for some specific frequencies. Particularly, errors at around 89 Hz in the case of the subplot (a-i) in Fig. 21 is related to the trough appearing at this frequency in the subplot (b-ii-1) in Fig. 4. On the other hand, results associated to half-space cases seems to behave differently. For these cases, distances between sources and collocation points larger than 0.5 m results in high errors of the new methodology, as seen in the subplots denoted by (a) and (b) in Fig. 22, which represent the results obtained for the cases of a solid cylinder and a thin shell, respectively. These cases are developed, both for the new method and the 2.5D FEM-BEM, in the basis of a Green's function calculation with the EDT toolbox considering a slowness associated to the wavenumber in the y direction logarithmically sampled from 10^{-7} to 10^{3} with 919 points. This is the sampling used in all the half-space Green's functions computations required for the results in previous sections of the present work. However, subplot (c) of Fig. 22 is related to the case of the thin shell structure when the half-space Green's functions in the new methodology are computed using a sampling for the slowness ranging between 10^{-11} to 10^{7} with 13240 samples, while the 2.5D FEM-BEM is based on the previous sampling scheme. The results obtained in subplot (c) are more likely the ones presented in full-space case which leads to the conclusion that the new methodology is more sensitive to the accuracy of the Green's functions than the 2.5D FEM-BEM. This finding turns the control methodology presented even more essential to ensure the correctness and the computational efficiency of the method, since a proper selection of the distance d results on accurate results of the method, even if the half-space Green's functions are computed using the same sampling scheme for the numerical integration.

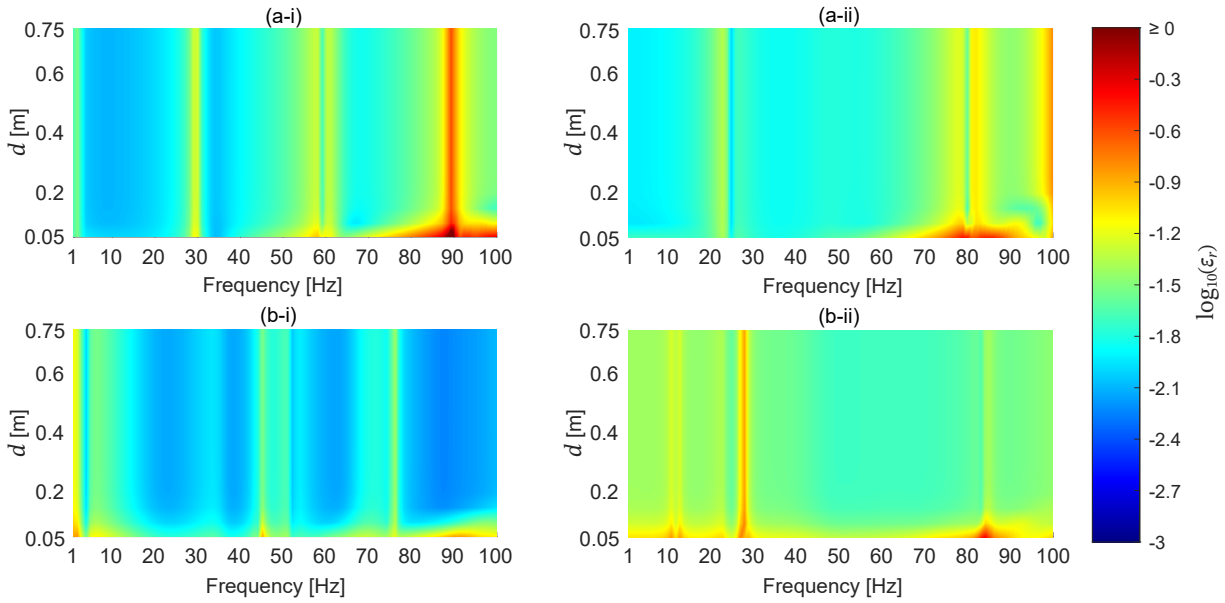

Figure 21: Relative error of the displacement Green's functions of the new methodology for the calculation examples in full-space, where (a) and (b) denote solid cylinder or thin shell structures, respectively, and (i) and (ii) represent the wavenumber of 0.1 rad/m and 1 rad/m, respectively.

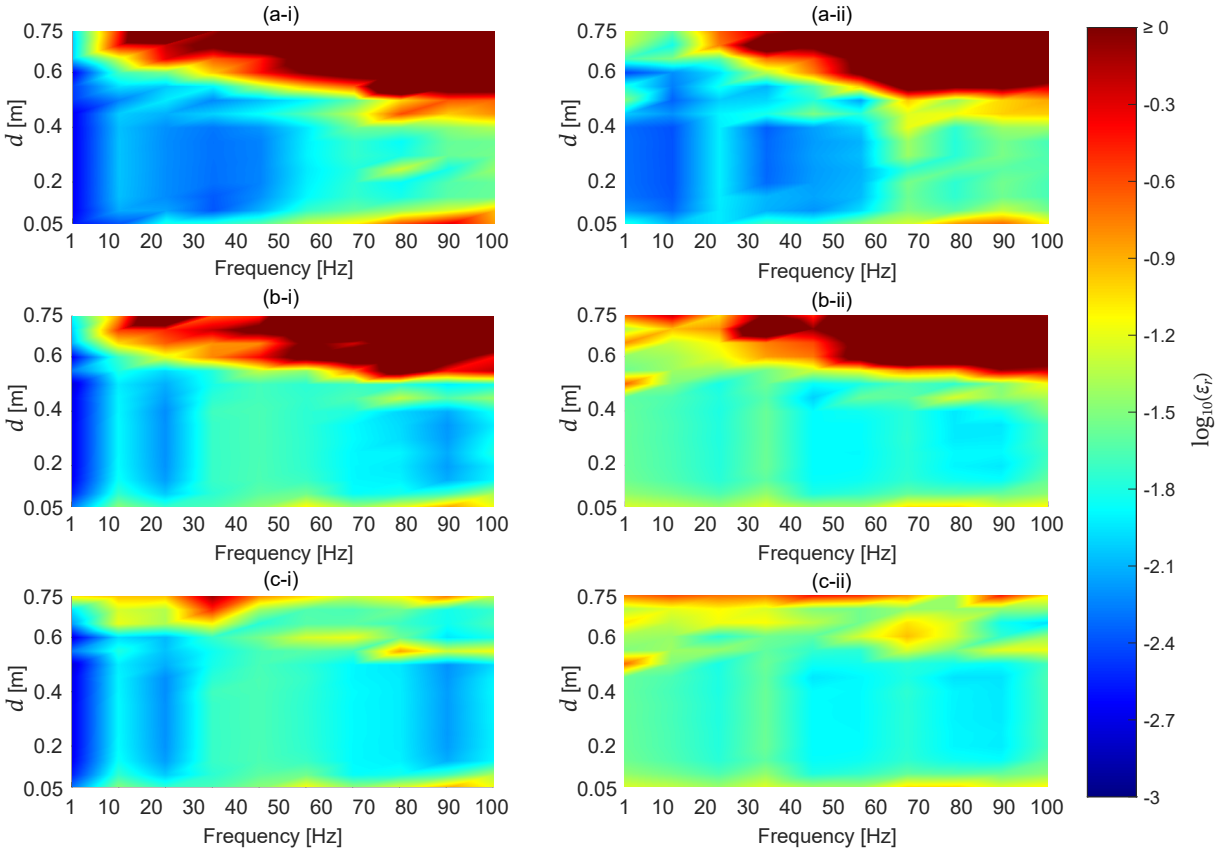

Figure 22: Relative error of the displacement Green's functions of the new methodology for the calculation examples in half-space, where (a), (b) solid cylinder and thin shell structures, respectively, and (i) and (ii) represent the wavenumber of 0.1 rad/m and 1 rad/m, respectively. The plots denoted by (c) are related to the case of the thin shell structure in which the used 2.5D Green's functions of the half-space are computed highly accurately.

6. Conclusions

The current study presents a methodology to deal with longitudinally invariant soil-structure interaction problems in elastodynamics. The method uses a 2.5D FEM-BEM approach to model structure and the locally surrounding soil and, then, uses a 2.5D MFS approach in elastodynamics to model the wave propagation through the soil. The new methodology is verified in terms of the displacement and traction Green's functions as well as the receptances and traction transfer functions up to frequencies of 100 Hz and 250 Hz. According to the results obtained in the previous sections, this method provides similar levels of accuracy than a full 2.5D FEM-BEM model of the soil-structure system and, moreover, spending a smaller amount computational time. Furthermore, the inclusion of the MFS as a post-processing tool has found to be very simple to be implemented. However, it is also found, as was expected, that the accuracy of the 2.5D FEM-BEM-MFS strongly depends on the accuracy of the boundary conditions obtained by 2.5D FEM-BEM method. Besides these general outcomes, this study has arisen other significant findings:

- A comparison between the new approach and the 2.5D FEM-BEM in terms of the computational efficiency has been provided. The results indicate that, for the calculation examples where the soil is modelled as a full-space medium, the time consumed by the new method follows a linear trend with the number of evaluation points, while the computational time associated to the 2.5D FEM-BEM method increases exponentially. For the half-space calculation examples, the improvement of the proposed methodology in terms of computational time is

also confirmed, although the improvement is not as large as in full-space problems. That is due to the numerical integration required for the evaluation of the 2.5D elastodynamic Green's functions in a half-space, in contrast to the analytical nature of the ones for full-space, and because of the particular computational performance of the algorithm used for their calculation.

- Cubic interpolation from the displacements on the boundary nodes to a larger set of collocation points has been found to be an interesting procedure, since it induces an enhancement of the results accuracy by adding no significant increment in the computational time of the full method. This improvement is shown by comparing the accuracy of the results obtained by taking 24 boundary nodes and 36 collocation points with respect to the case of 24 boundary nodes and 24 collocation points.
- A control technique that minimises the MFS error by optimising the distance between collocation points and virtual sources has been also presented. This control technique is demonstrated to be very useful in cases where the Green's functions have a semi-analytical nature, since the 2.5D MFS is found to be much more sensitive to the Green's functions accuracy than the 2.5D FEM-BEM when the response in evaluation points in the medium is computed. This sensitiveness is observed in the application of the control technique in half-space cases, where the 2.5D elastodynamic Green's functions computation requires a numerical integration, but, in contrast, it is not observed in the calculation examples embedded in a full-space, since the Green's functions for this case are analytical. From the results obtained, it is proposed a practical application of this control technique based only in few control points (located at the area where the final response is required) and some selected frequencies, in order not to compromise the computational efficiency of the whole method.

Acknowledgements

This research has been carried out with the financial support of Acoustical and Mechanical Engineering Laboratory (LEAM) of the Universitat Politècnica de Catalunya UPC and the project VIBWAY: Fast computational tool for railway-induced vibrations and re-radiated noise assessment, with reference RTI2018-096819-B-I00, supported by the Ministerio de Ciencia e Innovación, Retos de Investigación 2018. Second author would like to extend their gratitude to the financial support given by the project NVTRail: Noise and Vibrations induced by railway traffic in tunnels: an integrated approach, funded by FEDER funds through COMPETE2020 (Programa Operacional Competitividade e Internacionalizacão (POCI)) and by national funds (PIDDAC) through FCT/MCTES, with grant reference POCI-01-0145-FEDER-029577.

References

[1] Alves, C.J., 2009. On the choice of source points in the method of fundamental solutions. Engineering Analysis with Boundary Elements 33, 1348–1361. doi:10.1016/j.enganabound.2009.05.007.

[2] Amado-Mendes, P., Alves Costa, P., Godinho, L.M., Lopes, P., 2015. 2.5D MFS-FEM model for the prediction of vibrations due to underground railway traffic. Engineering Structures 104, 141–154. doi:10.1016/j.engstruct.2015.09.013.

[3] Amorosi, A., Boldini, D., di Lernia, A., 2017. Dynamic soil-structure interaction: A three-dimensional numerical approach and its application to the Lotung case study. Computers and Geotechnics 90, 34–54. doi:10.1016/j.compgeo.2017.05.016.

[4] Chen, C.S., Karageorghis, A., Li, Y., 2016. On choosing the location of the sources in the MFS. Numerical Algorithms 72, 107–130. doi:10.1007/s11075-015-0036-0.

[5] Clouteau, D., Cottereau, R., Lombaert, G., 2013. Dynamics of structures coupled with elastic media - A review of numerical models and methods. Journal of Sound and Vibration 332, 2415–2436. doi:10.1016/j.jsv.2012.10.011.

[6] De Oliveira Barbosa, J.M., Kausel, E., Azevedo, Á., Calçada, R., 2015. Formulation of the boundary element method in the wavenumber-frequency domain based on the thin layer method. Computers and Structures 161, 1–16. doi:10.1016/j.compstruc.2015.08.012.

[7] Forrest, J.A., Hunt, H.E.M., 2006a. A three-dimensional tunnel model for calculation of train-induced ground vibration. Journal of Sound and Vibration 294, 678–705. doi:10.1016/j.jsv.2005.12.032.

[8] Forrest, J.A., Hunt, H.E.M., 2006b. Ground vibration generated by trains in underground tunnels. Journal of Sound and Vibration 294, 706–736. doi:10.1016/j.jsv.2005.12.031.

[9] François, S., Schevenels, M., Galvín, P., Lombaert, G., Degrande, G., 2010. A 2.5D coupled FE–BE methodology for the dynamic interaction between longitudinally invariant structures and a layered halfspace. Computer Methods in Applied Mechanics and Engineering 199, 1536–1548. doi:10.1016/j.cma.2010.01.001.

[10] Galvín, P., François, S., Schevenels, M., Bongini, E., Degrande, G., Lombaert, G., 2010. A 2.5D coupled FE-BE model for the prediction of railway induced vibrations. Soil Dynamics and Earthquake Engineering 30, 1500–1512. doi:10.1016/j.soildyn.2010.07.001.

[11] Ghangale, D., Arcos, R., Clot, A., Cayero, J., Romeu, J., 2020. A methodology based on 2.5D FEM-BEM for the evaluation of the vibration energy flow radiated by underground railway infrastructures. Tunnelling and Underground Space Technology 101, 103392. doi:10.1016/j.tust.2020.103392.

[12] Ghangale, D., Colaço, A., Alves Costa, P., Arcos, R., 2019. A methodology based on structural FEM-BEM and acoustic BEM models in 2.5D for the prediction of re-radiated noise in railway-induced ground-borne vibration problems. Journal of Vibration and Acoustics 141, 1–14. doi:10.1115/1.4042518.

[13] Godinho, L., Amado-Mendes, P., Pereira, A., Soares, D., 2013. A coupled MFS-FEM model for 2-D dynamic soil-structure interaction in the frequency domain. Computers and Structures 129, 74–85. doi:10.1016/j.compstruc.2013.08.010.

[14] Godinho, L., Amado-Mendes, P., Tadeu, A., 2015. Meshless analysis of soil-structure interaction using an MFS-MLPG coupled approach. Engineering Analysis with Boundary Elements 55, 80–92. doi:10.1016/j.enganabound.2014.10.016.

[15] Gu, Y., Chen, W., Zhang, J., 2012. Investigation on near-boundary solutions by singular boundary method. Engineering Analysis with Boundary Elements 36, 1173–1182. doi:10.1016/j.enganabound.2012.01.006.

[16] He, C., Zhou, S., Di, H., Guo, P., Xiao, J., 2018. Analytical method for calculation of ground vibration from a tunnel embedded in a multi-layered half-space. Computers and Geotechnics 99, 149–164. doi:10.1016/j.compgeo.2018.03.009.

[17] He, C., Zhou, S., Di, H., Shan, Y., 2017. A 2.5-D coupled FE–BE model for the dynamic interaction between saturated soil and longitudinally invariant structures. Computers and Geotechnics 82, 211–222. doi:10.1016/j.compgeo.2016.10.005.

[18] Hon, Y., Wei, T., 2005. The method of fundamental solution for solving multidimensional inverse heat conduction problems. CMES - Computer Modeling in Engineering and Sciences 7, 119–132. doi:10.3970/cmes.2005.007.119.

[19] Hussein, M., François, S., Schevenels, M., Hunt, H., Talbot, J., Degrande, G., 2014. The fictitious force method for efficient calculation of vibration from a tunnel embedded in a multi-layered half-space. Journal of Sound and Vibration 333, 6996–7018. doi:10.1016/j.jsv.2014.07.020.

[20] International Organization for Standardization, 2005. ISO 14837-1. Mechanical vibration. Ground-borne noise and vibration arising from rail systems. Part 1: General Guidance.

[21] Kausel, E., Roësset, J.M., 1981. Stiffness matrices for layered soils. Bulletin of the Seismological Society of America 71, 1743–1761.

[22] Lombaert, G., Degrande, G., François, S., Thompson, D.J., 2015. Ground-Borne Vibration due to Railway Traffic: A Review of Excitation Mechanisms, Prediction Methods and Mitigation Measures, in: Noise and Vibration Mitigation for Rail Transportation Systems. Notes on Numerical Fluid Mechanics and Multidisciplinary Design. Springer, Berlin, Heidelberg, pp. 253–287.

[23] Lopes, P., Alves Costa, P., Calçada, R., Silva Cardoso, A., 2014. Influence of soil stiffness on building vibrations due to railway traffic in tunnels: Numerical study. Computers and Geotechnics 61, 277–291. doi:10.1016/j.compgeo.2014.06.005.

[24] Neumaier, A., 1998. Solving ill-conditioned and singular linear systems: a tutorial on regularization. Society for Industrial and Applied Mathematics 40, 636–666.

[25] Noori, B., Arcos, R., Clot, A., Romeu, J., 2018. A method based on 3D stiffness matrices in Cartesian coordinates for computation of 2.5D elastodynamic Green's functions of layered half-spaces. Soil Dynamics and Earthquake Engineering 114, 154–158. doi:10.1016/j.soildyn.2018.07.031.

[26] Schevenels, M., François, S., Degrande, G., 2009. EDT: An ElastoDynamics Toolbox for MATLAB. Computers and Geosciences 35, 1752–1754. doi:10.1016/j.cageo.2008.10.012.

[27] Sheng, X., Jones, C.J., Thompson, D.J., 2005. Modelling ground vibration from railways using wavenumber finite- and boundary-element methods. Proceedings of the Royal Society A: Mathematical, Physical and Engineering Sciences 461, 2043–2070. doi:10.1098/rspa.2005.1450.

[28] Sun, Y., Marin, L., 2017. An invariant method of fundamental solutions for two-dimensional isotropic linear elasticity. International Journal of Solids and Structures 117, 191–207. doi:10.1016/j.ijsolstr.2017.02.022.

[29] Tadeu, A., António, J., Godinho, L., 2009. Defining an accurate MFS solution for 2.5D acoustic and elastic wave propagation. Engineering Analysis with Boundary Elements 33, 1383–1395. doi:10.1016/j.enganabound.2009.06.007.

[30] Tadeu, A.J.B., Kausel, E., 2000. Green's functions for two-and-a-half-dimensional elastodynamic problems. Journal of Engineering Mechanics - ASCE 126, 1093–1097.

[31] Wang, L., Wang, Z., Qian, Z., 2017. A meshfree method for inverse wave propagation using collocation and radial basis functions. Computer Methods in Applied Mechanics and Engineering 322, 311–350. doi:10.1016/j.cma.2017.04.023.

[32] Wong, K.Y., Ling, L., 2011. Optimality of the method of fundamental solutions. Engineering Analysis with Boundary Elements 35, 42–46. doi:10.1016/j.enganabound.2010.06.002.